

## Drug Delivery

## Anti-cancer Applications of Titanocene-Functionalised Nanostructured Systems: An Insight into Cell Death Mechanisms

Jesús Ceballos-Torres,<sup>[a]</sup> Piroska Virag,<sup>[b]</sup> Mihai Cenariu,<sup>[c]</sup> Sanjiv Prashar,<sup>[a]</sup> Mariano Fajardo,<sup>[a]</sup> Eva Fischer-Fodor,<sup>\*[b]</sup> and Santiago Gómez-Ruiz<sup>\*[a]</sup>

**Abstract:** A series of alkenyl-substituted titanocene compounds have been supported on the mesoporous silica-based material KIT-6. The corresponding functionalised materials were completely characterised by different techniques (solid-state multinuclear NMR spectroscopy, IR spectroscopy, N<sub>2</sub> adsorption–desorption isotherms, X-ray fluorescence and diffraction, SEM and TEM) to observe the incorporation of the titanocene derivatives on the external surface of the material KIT-6. Both the titanocene compounds and the materials were tested in vitro against a wide variety of human cancer and normal cell lines. A very high cytotoxicity of the synthesised titanocene derivatives (IC<sub>50</sub> values in the range of those described in the literature for the most active cytotoxic titanocene compounds), with selectivity towards cancer cell lines was observed. The cytotoxic activity of the

materials is the highest reported to date for titanocene-functionalised materials. In addition, higher Ti uptake (from 4 to 23% of the initial amount of Ti) of the cells treated with materials was observed with respect to those treated with “free” titanocene derivatives (which gave Ti uptake values from 0.4 to 4.6% of the initial amount of Ti). Additional experiments with the titanocene derivatives and the functionalised materials revealed that changes to the morphological and functional dynamics of apoptosis occurred when the active titanocene species were incorporated into mesoporous materials. In addition, the materials could induce programmed cell death in tumour cell populations by impairing the damaged DNA repair mechanisms and by upregulation of intrinsic and extrinsic apoptotic signalling pathways.

## Introduction

Chemotherapeutic treatments based on metallodrugs have traditionally used platinum complexes due to their excellent cytotoxic properties.<sup>[1]</sup> However, the relatively high number of side effects associated with platinum treatments has opened up interest in the use of other metal complexes with similar anti-neoplastic properties, but with higher potential application in humans. Thus, in recent years, outstanding results have been obtained by using alternative metal complexes in preclinical trials in vitro, although most of them have not been translated into comparable developments in vivo due to problems in their administration, which does not permit formulations with high selectivity and minimum collateral damage.<sup>[2–7]</sup>

[a] J. Ceballos-Torres, Dr. S. Prashar, Prof. M. Fajardo, Dr. S. Gómez-Ruiz  
Departamento de Química Inorgánica y Analítica, E.S.C.E.T.  
Universidad Rey Juan Carlos, 28933 Móstoles, Madrid (Spain)  
E-mail: santiago.gomez@urjc.es

[b] Dr. P. Virag, Dr. E. Fischer-Fodor  
Research Department, “I.Chiricuta” Oncology Institute  
Cluj Napoca 400015 (Romania)  
E-mail: fischer.eva@iocn.ro

[c] Dr. M. Cenariu  
Biotechnology Research Center  
University of Agricultural Science and Veterinary Medicine  
Cluj Napoca, 400372 (Romania)

Supporting information for this article is available on the WWW under  
<http://dx.doi.org/10.1002/chem.201400300>.

Most of the problems associated with the application of these metal-based drugs in humans are due to the low effectiveness of transport processes of active species to the biological target. For this reason, the scientific community has now focused its efforts on the design of novel therapeutic technologies mainly based on nanostructured materials, which may act as vectors for the delivery of the metallodrug or simply as a protector of the active species for the enhancement of its anti-cancer action.<sup>[8,9]</sup>

In this context, many different systems have been used as scaffolds for loading with metal-based drugs. Macromolecular systems based on curcubit[*n*]urils and cyclodextrins have already been successfully used in preclinical trials, especially with platinum drugs and metallocene-based therapeutic complexes.<sup>[10–13]</sup> Liposomes and lipid nanocapsules have also been used as vehicles for the delivery of hydrophobic drugs to the desired biological target, although, again, these systems have only been loaded with platinum complexes<sup>[14]</sup> or ferrocene derivatives.<sup>[15]</sup> Other approaches have focused on alternative macromolecular systems, such as proteins, for example, human serum albumin<sup>[16–18]</sup> or apoferritin,<sup>[19]</sup> and, recently, even polynuclear organometallic compounds have been used as encapsulators of platinum and palladium complexes with cytotoxic activity.<sup>[20]</sup> Some additional studies have been performed by using nanosystems based on carbon nanotubes<sup>[21–23]</sup> and polymeric nanoparticles.<sup>[24–26]</sup>

However, our interest is focused on the use of ceramic materials, such as calcium phosphate, hydroxyapatite or mesoporous silicas, because they can be used as components of synthetic hard tissues, such as bone fillers or prostheses. Thus, functionalisation of these materials with metallo drugs allows the formation of systems that have the potential to be applied, after surgery, for the in situ treatment of bone tumours with the aim of avoiding the reappearance of the tumour in the same area.<sup>[27–29]</sup> With this objective, several groups have focused their research on the adsorption, desorption and therapeutic properties of cisplatin and other platinum compounds towards two biomimetic synthetic hydroxyapatite-based nanocrystalline materials with different morphologies and physicochemical properties.<sup>[30,31]</sup> For mesostructured silica-based materials, the first study with metal complexes was performed for the encapsulation of cisplatin with the help of CdS caps,<sup>[32]</sup> and subsequently, only our group has worked with other metal-based drugs, namely, titanocene derivatives, and observed that all functionalised surfaces exhibited in vitro cytotoxicity against a wide variety of human cancer cells.<sup>[33–36]</sup> However, these studies did not clarify the mechanism of action of the titanocene-functionalised materials. Nevertheless, the results showed that the incorporation of titanocene derivatives on mesoporous silica-based particles was a viable alternative for the administration of titanocene derivatives and may help in the enhancement of their therapeutic properties by overcoming the problems of hydrophobicity associated with these compounds.<sup>[37,38]</sup>

Herein, we report novel insights into the mechanisms of action of titanocene-functionalised mesoporous silica-based materials. We have prepared a series of alkenyl-substituted titanocene compounds that have very high cytotoxic activity (comparable to that of titanocene-Y, which is one of the most potent metallo drugs based on titanium). Their corresponding mesoporous materials present much higher cytotoxic activity (lower  $M_{50}$  or  $Ti-M_{50}$  values) and selectivity than similar nanostructured systems functionalised with titanocene derivatives.<sup>[33–36]</sup>

In addition, we show that titanium-functionalised materials act as Trojan horses for the incorporation of titanium active species into the cells, leading to much higher quantities of titanium uptake in cells, than that observed with “free” titanocene derivatives. These results indicate that transport processes (either active or passive) of “free” titanocene derivatives to the cell are less effective than those of the titanocene-functionalised materials.

Finally, we report additional apoptotic experiments, such as the study of the apoptosis induction capacity, an evaluation of the modulator effect on intrinsic apoptotic pathway and apoptosis regulation at DNA level. We observed that the dynamics of apoptotic morphological and functional changes were modified significantly when the active titanocene species were incorporated onto mesoporous materials. These materials are also able to program cell death in tumour cell populations by impairing the damaged DNA repair mechanisms and by up-regulation of intrinsic and extrinsic apoptotic signalling pathways.

## Results and Discussion

### Synthesis and characterisation of titanocene complexes

#### Synthesis and spectroscopic characterisation of titanocene(IV) complexes

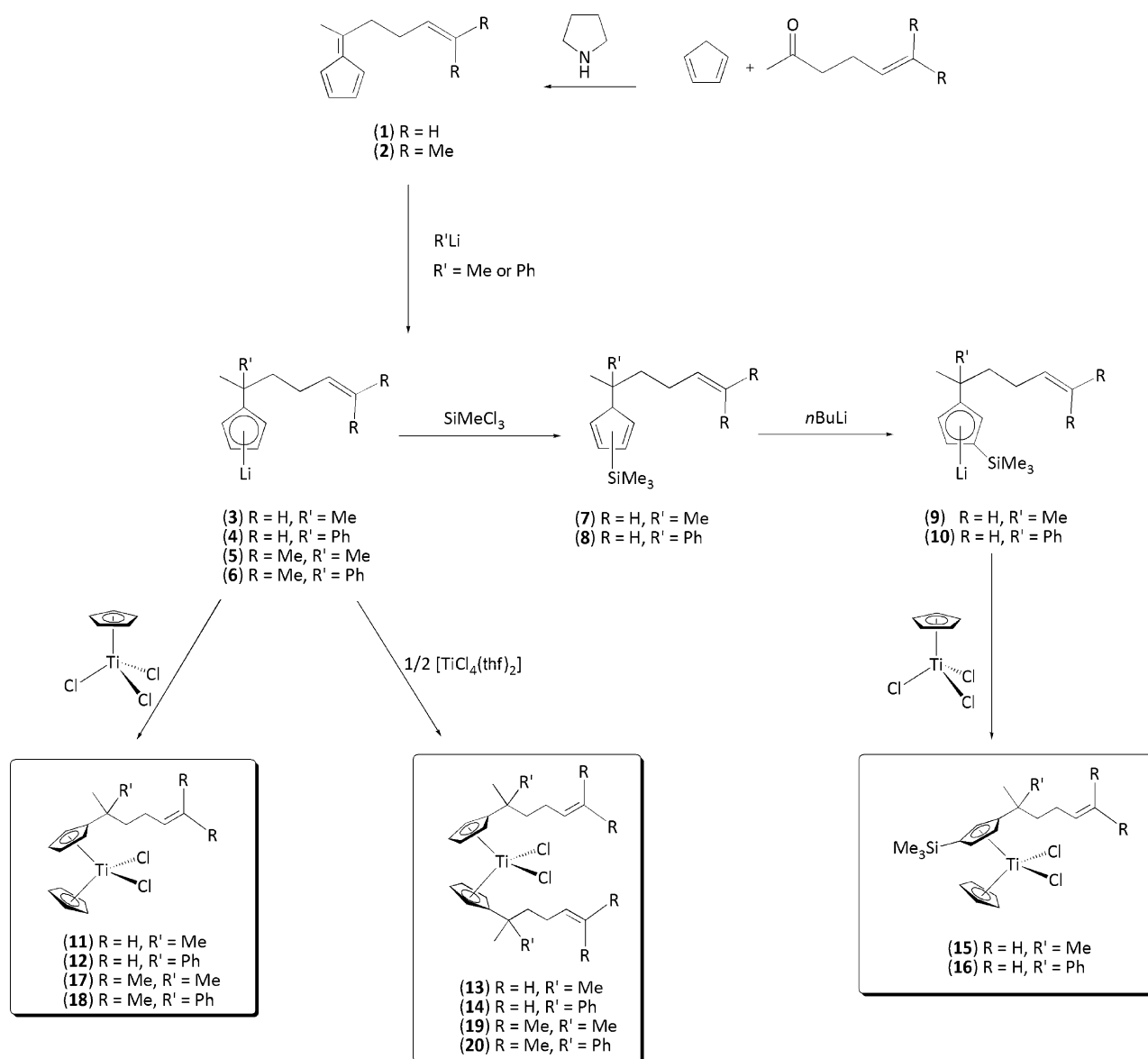
The synthesis of the titanocene(IV) complexes (**11–20**) was performed according to the synthetic routes described in Scheme 1, starting from the corresponding titanium precursor ( $[Ti(\eta^5-C_5H_5)Cl_3]$  or  $[TiCl_4(thf)_2]$ ) and the stoichiometric ratio of the corresponding lithium cyclopentadienide derivative (**4**, **5**, **6**, **9** or **10**; Scheme 1 and the Supporting Information). Complexes **11–20** were characterised by multinuclear NMR spectroscopy, FTIR spectroscopy, mass spectrometry and elemental analysis.

NMR spectroscopy of compounds **14** and **20** revealed the formation of the expected *rac* and *meso* isomers (1:1 ratio), which arose from the presence of two chiral centres. In addition, it is important to note the existence of planar chirality due to the disubstitution of the cyclopentadienyl (Cp) ring in **15** and **16**. In the case of compound **16**, the planar chirality together with the chiral centre of the alkenyl substituent leads to the formation of two isomers. NMR spectroscopy showed that these isomers were present in a 1:1 ratio. For further information about the possible isomers in **14**, **16** and **20**, see Figures S1 and S2 in the Supporting Information.

As a general rule for asymmetric titanocene complexes with mixed rings (**11**, **12**, **15**, **16**, **17** and **18**), the  $^1H$  NMR spectra showed a singlet assigned to the unsubstituted Cp ring between  $\delta = 6.1$  and 6.6 ppm. In addition, a set of two signals corresponding to the protons of the substituted Cp ring between  $\delta = 6.0$  and 6.6 ppm was observed for **11**, **12**, **17** and **18**. In the case of complexes **15** and **16**, which have a 1,3-disubstituted Cp ligand, three signals corresponding to the three protons of the Cp ring between  $\delta = 6.0$  and 6.7 ppm and a singlet at  $\delta \approx 0.2$  ppm, assigned to the protons of the trimethylsilyl group, were observed.

A set of signals associated with the alkenyl fragments was also observed in the  $^1H$  NMR spectra of **11–20**. Thus, titanocene compounds **11**, **13** and **15** showed a singlet at about  $\delta = 1.20$  ppm, due to two methyl groups substituting the carbon atom bonded to the Cp ring, and five sets of signals, two corresponding to the methylene protons (two multiplets between  $\delta = 1.5$  and 2.0 ppm), one corresponding to the proton of the C- $\delta$  (a multiplet at  $\delta = 5.6$  ppm) and two for the terminal olefinic protons (multiplets at  $\delta \approx 4.7$  and 4.9 ppm). Compounds **12**, **14** and **16** showed an additional set of three aromatic proton signals assigned to the phenyl ring protons.

For complexes **17** and **19**, a singlet due to the two methyl groups substituting the carbon atom adjacent to the Cp ring was observed at about  $\delta = 1.2$  ppm. In addition, five sets of signals, two corresponding to the  $CH_2$  methylene protons (two multiplets between  $\delta = 1.4$  and 1.9 ppm), one corresponding to the alkenylic proton of the C- $\delta$  (triplet at  $\delta \approx 5.0$  ppm) and two singlets corresponding to the protons of the terminal methyl groups (between  $\delta = 1.4$  and 1.7 ppm), were observed.



Scheme 1. Synthesis of titanocene compounds 11–20.

Complexes **18** and **20** showed an additional set of three aromatic proton signals assigned to the phenyl ring protons.

As previously mentioned, in the cases of compounds **14**, **17** and **20**, due to the existence of two isomers all of the observed signals were twinned.

The <sup>13</sup>C{<sup>1</sup>H} NMR spectra of **11–20** showed the expected signals. The mass spectra showed the molecular ion peak and other peaks corresponding to typical fragmentations of the molecules.

#### X-ray structure of **17** and **18**

Compounds **17** (Figure 1) and **18** (Figure 2) crystallise in the monoclinic space groups *P*2<sub>1</sub>/*n* and *P*2<sub>1</sub>/*c*, respectively, both with four molecules in the unit cell. Both compounds crystallise in centrosymmetric space groups; compound **18** crystallises as a racemate. Table 1 lists crystallographic details and

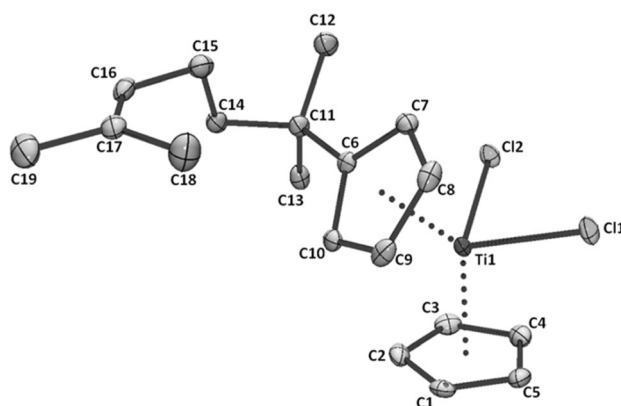
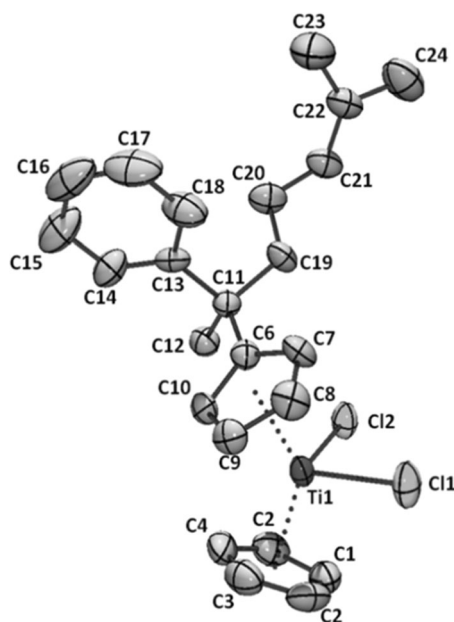


Figure 1. X-ray molecular structure and atom labelling scheme of compound **17** with thermal ellipsoids at 50% probability. Hydrogen atoms have been omitted for clarity.<sup>[60]</sup>



**Figure 2.** X-ray molecular structure and atom labelling scheme of compound **18** with thermal ellipsoids at 50% probability. Hydrogen atoms have been omitted for clarity.<sup>[60]</sup>

Table 1. Crystallographic data of <b>17</b> and <b>18</b>		
	<b>17</b>	<b>18</b>
formula	C <sub>19</sub> H <sub>26</sub> Cl <sub>2</sub> Ti	C <sub>24</sub> H <sub>28</sub> Cl <sub>2</sub> Ti
M <sub>r</sub>	373.20	435.26
T [K]	298(2)	298(2)
crystal system	monoclinic	monoclinic
space group	P2 <sub>1</sub> /n	P2 <sub>1</sub> /c
a [pm]	653.10(13)	1138.2(13)
b [pm]	1892.4(4)	1248.1(12)
c [pm]	1457.1(3)	1606(2)
α [°]	90	90
β [°]	100.37(3)	110.49(5)
γ [°]	90	90
V [Å <sup>3</sup> ]	1771.5(6)	2138(4)
Z	4	4
crystal size [mm <sup>3</sup> ]	0.20 × 0.15 × 0.10	0.10 × 0.06 × 0.04
ρ <sub>calcd</sub> [mg m <sup>-3</sup> ]	1.399	1.352
F(000)	784	912
absorption coefficient [mm <sup>-1</sup> ]	0.779	0.657
hkl range	-7 ≤ h ≤ 7, -21 ≤ k ≤ 21, -16 ≤ l ≤ 16	-12 ≤ h ≤ 12, -14 ≤ k ≤ 14, -18 ≤ l ≤ 18
2θ <sub>max</sub> [°]	46.60	47.42
reflins collected/unique	21 730/2567	28 862/3166
R(int)	0.0413	0.1845
data/restraints/parameters	2567/0/203	3166/0/247
GoF on F <sup>2</sup>	1.031	1.040
R <sub>1</sub> /wR <sub>2</sub> [I > 2σ(I)]	0.0232/0.0527	0.0763/0.1737
R <sub>1</sub> /wR <sub>2</sub> (all data)	0.0277/0.0547	0.1197/0.1946
largest diff. peak/hole [e Å <sup>-3</sup> ]	0.253/-0.183	0.561/-0.343

Table 2 gives selected bond lengths and angles of **17** and **18**. The molecular structures reveal a tetrahedral geometry about the titanium atom with coordination of the Cp rings in an η<sup>5</sup> manner. The bond lengths between titanium and the Cp

Table 2. Selected bond lengths (pm) and angles (°) for <b>17</b> and <b>18</b> .		
	<b>17</b>	<b>18</b>
Ti1–Cent1 <sup>[a]</sup>	207.0(2)	205.4(8)
Ti1–Cent2 <sup>[a]</sup>	207.4(2)	208.5(7)
av Ti1–C(C1–C5) <sup>[b]</sup>	238.1(2)	236.4(8)
av Ti1–C(C6–C10) <sup>[b]</sup>	239.5(2)	239.7(7)
Ti1–C1	235.7(2)	238.0(8)
Ti1–C2	237.1(2)	236.7(8)
Ti1–C3	239.4(3)	233.2(8)
Ti1–C4	238.9(2)	234.6(7)
Ti1–C5	239.3(2)	239.5(8)
Ti1–C6	245.8(2)	248.3(7)
Ti1–C7	241.8(2)	242.1(7)
Ti1–C8	238.1(2)	237.6(7)
Ti1–C9	233.2(2)	233.8(7)
Ti1–C10	238.5(2)	236.8(6)
Ti1–Cl1	238.03(8)	235.3(3)
Ti1–Cl2	235.82(9)	231.9(3)
C15–C16	1.500(3)	1.35(2)
C16–C17	1.324(3)	1.36(2)
C17–C18	1.497(3)	1.40(2)
C17–C19	1.501(3)	
C20–C21		1.49(1)
C21–C22		1.296(9)
C22–C23		1.51(1)
C22–C24		1.48(2)
Cent1–Ti–Cent2	131.8(2)	132.8(9)
Cl1–Ti1–Cent1	105.5(2)	106.3(9)
Cl1–Ti1–Cent2	107.1(2)	105.6(9)
Cl2–Ti1–Cent1	106.1(1)	105.0(9)
Cl2–Ti1–Cent2	106.7(2)	107.6(9)
Cl1–Ti1–Cl2	92.82(2)	92.4(1)
C15–C16–C17	127.7(2)	121.4(9)
C16–C17–C18	124.7(2)	118.4(9)
C16–C17–C19	121.8(2)	
C18–C17–C19	113.6(2)	
C20–C21–C22		129.5(7)
C21–C22–C23		125.1(8)
C21–C22–C24		120.9(8)
C23–C22–C24		114.0(7)

[a] Cent1 and Cent2 are the centroids of C1–C5 and C6–C10, respectively.  
[b] The average distance between Ti1 and the carbon atoms of the C<sub>5</sub> ring of the corresponding Cp moiety.

carbon atoms of titanocene complexes **17** and **18** vary from about 233 to 248 pm. The longest Ti–C bond lengths are observed for the substituted carbon atom of the Cp ring (C6). The Ti–Cent distances in **17** and **18** are between 205 and 209 pm and the Cent–Ti–Cent angles are about 132°; these values are in the expected range for titanocene derivatives.<sup>[39–41]</sup> In addition, the Cl1–Ti1–Cl2 angles of about 92° are similar, and comparable with those recorded for the X-ray crystal structures of other related titanocene complexes.<sup>[39–41]</sup>

The C17–C18 and C21–C22 bond lengths for the double bonds of the alkenyl chain of **17** and **18**, respectively, have values of about 130 pm and are in agreement with reported structures of other titanocene complexes with alkenyl substituents.<sup>[42–44]</sup>

## Synthesis and characterisation of materials incorporating titanocene complexes (K11–K20)

### Synthesis and characterisation of KIT-6

Mesoporous material KIT-6 was prepared according to the synthetic method described by Ryoo and co-workers (see the Supporting Information).<sup>[45]</sup> The physical parameters of nitrogen adsorption–desorption isotherms (Figure 3) of this material

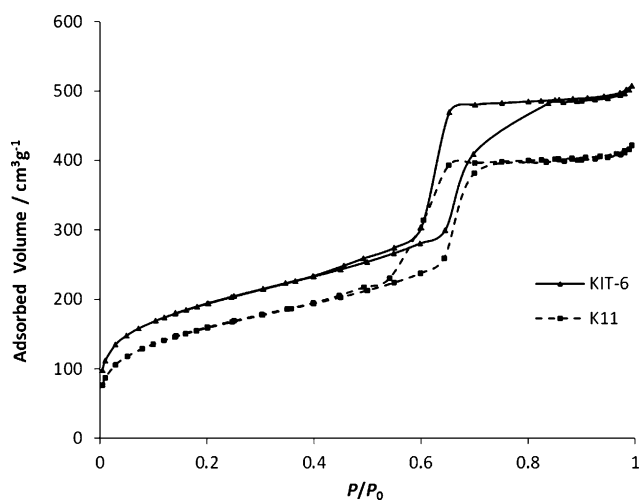
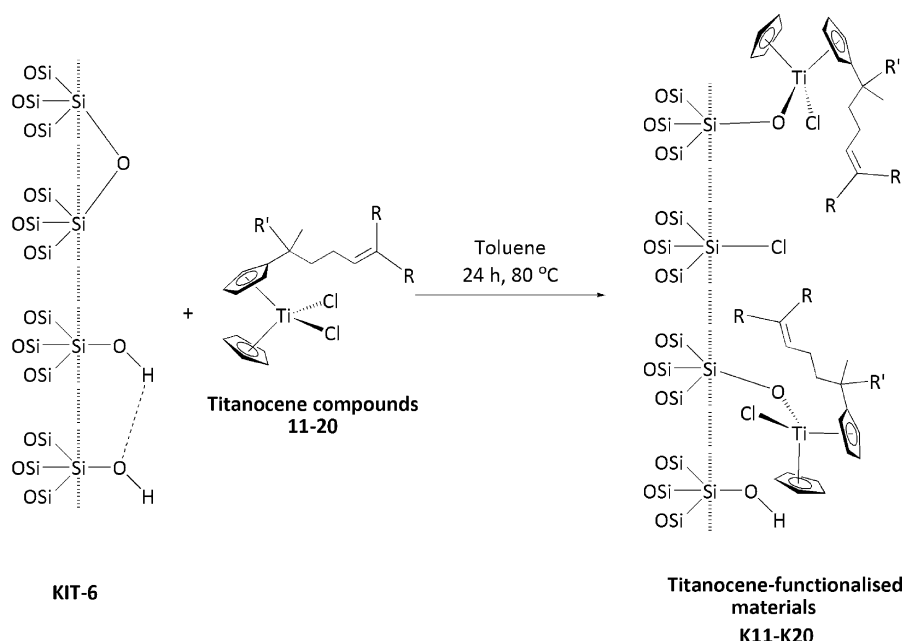


Figure 3. Nitrogen adsorption/desorption isotherms of KIT-6 and K11.

showed a typical type IV isotherm (according to the IUPAC classification)<sup>[46]</sup> with an H2 hysteresis loop. In addition, synthesised KIT-6 had a BET surface area ( $S_{\text{BET}}$ ) of  $694 \text{ m}^2 \text{ g}^{-1}$ , an average pore diameter of  $63.7 \text{ \AA}$  and an average pore volume of  $0.76 \text{ cm}^3 \text{ g}^{-1}$ ; these values are typical for mesostructured materials. The low-angle XRD pattern of KIT-6 (which has a three-dimensional cubic symmetry ( $la3d$ )) gave an intense peak at  $2\theta = 0.95^\circ$  (assigned to the (211) plane) and two very weak peaks at  $2\theta = 1.65$  and  $1.90^\circ$  (indexed as (220) and (320));<sup>[45,47]</sup> see Figure S3 in the Supporting Information).

Additionally, analysis of this material by FTIR spectroscopy gave a spectrum with a broad band between  $3400$  and  $3200 \text{ cm}^{-1}$ , which was attributed to O–H stretching of the silanol groups of the surface and the remaining adsorbed water molecules. The stretching band of the Si–O bonds was observed at  $805 \text{ cm}^{-1}$  and a broad strong band between  $1100$  and  $1250 \text{ cm}^{-1}$ , corresponding to the siloxane groups (Si–O–Si), was also recorded.



Scheme 2. Synthesis of titanocene-functionalised materials K11–K20.

Finally, characterisation of this material by  $^{29}\text{Si}$  MAS NMR spectroscopy showed typical  $\text{Q}^4$  ( $\text{Si}(\text{OSi})_4$ ),  $\text{Q}^3$  ( $\text{Si}(\text{OSi})_3(\text{OH})$ ) and  $\text{Q}^2$  ( $\text{Si}(\text{OSi})_2(\text{OH})_2$ ) signals at  $\delta = -112$ ,  $-104$  and  $-92$  ppm, respectively.

### Synthesis and characterisation of titanocene-functionalised materials

The synthesis of the titanocene-functionalised materials was performed by grafting of the different titanocene compounds synthesised in this study (11–20) on dehydrated (at  $500^\circ\text{C}$ ) KIT-6 mesoporous silica. This reaction is very simple and consists of the treatment of the dehydrated material overnight with a solution of the titanocene compounds in toluene under reflux (Scheme 2).

Because the non-functionalised KIT-6 has a low concentration of hydroxyl groups from silanol moieties due to its treatment at high temperature, the only possible reactions between titanocene derivatives and KIT-6 mesoporous silica are those involving the chlorine atoms of the titanocene complexes, either with the acidic silanol groups or with the reactive siloxane bridges, to give  $\mu$ -oxo surface species, as observed in previous reports (Scheme 2).<sup>[33–36]</sup> Notably, adsorbed titanocene complexes may also be located in the pore of the corresponding materials.

Following our previous work on the functionalisation reactions of mesoporous silicas with titanocene derivatives, graft-

ing reactions were performed by using a theoretical 5 wt% of Ti.<sup>[33–36]</sup> From data obtained by X-ray fluorescence, values of Ti wt% for functionalised surfaces K11–K20 are between 1.20 and 4.85%, with most of the values falling between 2 and 3%. It is worth noting the unusually high functionalisation rate of K20 with a Ti wt% of 4.85 (Table 3). The relatively low Ti

**Table 3.** Physical parameters of unmodified KIT-6 and of the modified materials **K11–K20** measured by N<sub>2</sub> adsorption–desorption isotherms and percentage of Ti grafted on the silica support in surfaces **K11–K20**, as measured by X-ray fluorescence.

	BET surface area [m <sup>2</sup> g <sup>-1</sup> ] <sup>[a]</sup>	Total pore volume [cm <sup>3</sup> g <sup>-1</sup> ]	Pore diameter (BJH) <sup>[a]</sup> [Å]	Ti [wt %]
<b>KIT-6</b>	694	0.76	63.7	–
<b>K11</b>	575	0.63	63.6	2.13
<b>K12</b>	592	0.67	63.7	1.20
<b>K13</b>	610	0.68	63.7	2.17
<b>K14</b>	469	0.42	68.7	2.26
<b>K15</b>	561	0.44	63.8	3.06
<b>K16</b>	532	0.59	64.3	2.43
<b>K17</b>	492	0.44	64.3	2.23
<b>K18</b>	442	0.41	63.9	2.00
<b>K19</b>	365	0.37	63.9	2.43
<b>K20</b>	348	0.33	64.2	4.85

[a] BJH = Barrett, Joyner and Halenda.

amount in the functionalised materials may be due either to the saturation of the surface or to the weak basicity of both chloro ligands of the titanocene complexes and the weak acidity of Si–OH groups of the KIT-6 mesoporous material.

For **K11–K20**, the functionalisation rate (Ti wt%) is somewhat higher than those obtained in previous studies of the functionalisation of MCM-41, SBA-15, HMS and MSU-2 with titanocene derivatives, for which a maximum loading of the metallocene complex on the mesoporous surfaces was always lower than 2.0% of the metal, even when starting from high metal/SiO<sub>2</sub> ratios.<sup>[33–36]</sup>

The physical parameters of nitrogen adsorption–desorption isotherms, such as BET surface area ( $S_{\text{BET}}$ ), average pore diameter, average pore volume, and wall thickness, for unmodified KIT-6 and the modified materials **K11–K20** were measured (Figure 3).

Typical type IV isotherms (according to the IUPAC classification)<sup>[46]</sup> with an H2 hysteresis loop were observed; this indicated the mesoporous nature of all of the studied materials. Capillary condensation of nitrogen within the uniform mesopore structure, as indicated by the increase in the adsorbed volume at a relative pressure ( $P/P_0$ ) of about 0.4, was observed for all studied surfaces. The inflection position shifted slightly towards lower relative pressures after functionalisation. Interestingly, a decrease in the surface area and pore volume of materials **K11–K20** was observed on direct comparison with the corresponding non-functionalised material (KIT-6; Table 3). The pore size distribution in all materials is very narrow, both before and after functionalisation with the titanocene derivatives (see Figures S4 and S5 in the Supporting Information). However, the pore diameter seems to be unaffected after the functionalisation reactions for KIT-6-based materials, contrary to that reported for the functionalisation of MCM-41, SBA-15, HMS and MSU-2, which showed a significant decrease of the pore diameter (Table 3). Thus, it seems plausible that for **K11–K20** only a very low amount of the titanocene derivative is located in the pore of the materials and the major part of the grafted titanocene compound is located on the external sur-

face of the mesoporous scaffold. The difference in the location of the titanocene derivative in **K11–K20** with KIT-6 as the support, compared with MCM-41, SBA-15, HMS and MSU-2 materials,<sup>[33–36]</sup> may be associated either with the higher pore diameter of free KIT-6 (of almost 70 Å) or with a higher number of silanol groups on the external surface, which is typical in KIT-6. These two textural properties of KIT-6 may minimise the interactions between the silanol groups of the pores on direct comparison with the silanol groups of the external surface, forcing functionalisation onto the external surface of the material.

In addition, all materials were characterised by powder X-ray diffraction, which gave low-angle patterns of KIT-6. The intensity of the peaks of materials **K11–K20** is lower than that of free KIT-6; this is probably due to blocking of the dispersion centres by the titanocene derivatives (see Figure S3 in the Supporting Information). Thus, the diffractograms displayed one intense peak at  $2\theta \approx 0.95^\circ$ , which can be indexed as (211). However, the two weak reflections at  $2\theta \approx 1.65$  and  $1.9^\circ$  (corresponding to (220) and (320), respectively) were barely observed due to lowering of their intensity by functionalisation with the metal complex.

Incorporation of the titanocene derivatives in the mesoporous scaffold was also confirmed by FTIR spectroscopy. All functionalised materials **K11–K20** showed, in addition to the bands of KIT-6, characteristic weak bands for C–H stretching vibrations between 3000 and 2800 cm<sup>-1</sup> and bending vibration bands at about 1400 cm<sup>-1</sup> due to the Cp ligands (for further information, see Figures S6 and S7 in the Supporting Information).

In addition, characterisation by multinuclear solid-state NMR spectroscopy confirmed functionalisation of the materials with the corresponding titanocene derivatives. The <sup>1</sup>H MAS NMR spectra of all materials showed expected signals corresponding to the different protons of the grafted titanocene complex. In each case, a broad signal assigned to protons situated in the sp<sup>3</sup>-carbon atoms of the alkenyl fragment was observed between  $\delta = 1.5$  and 4 ppm, whereas the protons of the sp<sup>2</sup>-carbon atoms (Cp ligands and those of the C=C double bond of the alkenyl fragment) were recorded between  $\delta = 4$  and 7 ppm. Moreover, in the special case of the materials **K12**, **K14**, **K16**, **K18** and **K20**, which contain phenyl groups, an additional signal above  $\delta = 7$  ppm was recorded due to the resonance of the aromatic protons of the phenyl groups. An additional signal between  $\delta = 0$  and 1 ppm, corresponding to the protons of the trimethylsilyl group, was observed for the materials **K15** and **K16**. Figure 4 shows the <sup>1</sup>H MAS NMR spectrum of **K16**.

The <sup>13</sup>C CP MAS NMR spectra showed different sets of signals, depending on the carbon atoms present in the grafted titanocene complex. Thus, the sp<sup>3</sup>-carbon atoms of the alkenyl fragment gave signals between  $\delta = 10$  and 40 ppm for all materials; the quaternary carbon atom was generally observed above  $\delta = 40$  ppm. In addition to these signals, resonances corresponding to the sp<sup>2</sup>-carbon atoms of the Cp, phenyl rings and alkenyl fragments were normally observed between  $\delta = 110$  and 140 ppm (Figure 5). Finally, for materials **K15** and **K16**, the resonance due to the carbon atom of the trimethylsilyl group was recorded at  $\delta = -2.6$  and  $-3.4$  ppm, respectively.

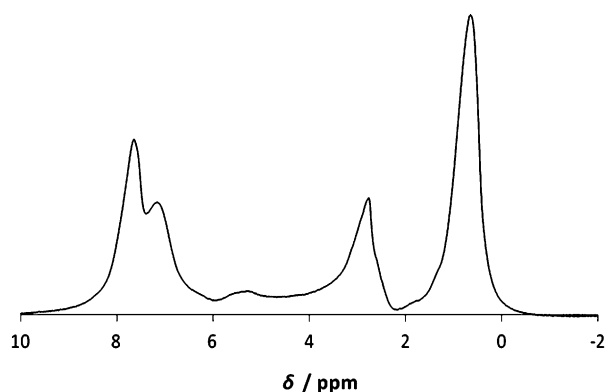


Figure 4.  $^1\text{H}$  MAS NMR spectrum of material K16.

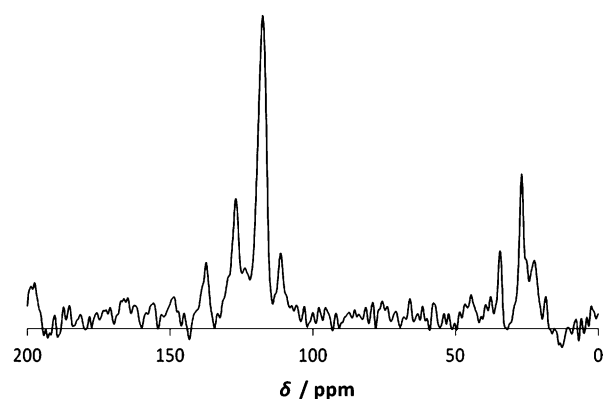


Figure 5.  $^{13}\text{C}$  CP MAS NMR spectrum of material K11.

In addition, the  $^{29}\text{Si}$  MAS NMR spectra of the functionalised materials (K11–K20) showed signals corresponding to the different  $Q^n$  sites of the mesoporous structure, which were also observed for the non-functionalised material. However, a drastic decrease in the intensity of these signals was observed in all materials relative to those of free KIT-6, as a consequence of functionalisation with the titanocene derivative (Figure 6).

Finally, SEM and TEM were used to explore the morphology of the studied materials. Results revealed that K11–K20 were aggregates of mesoporous small particles without a defined

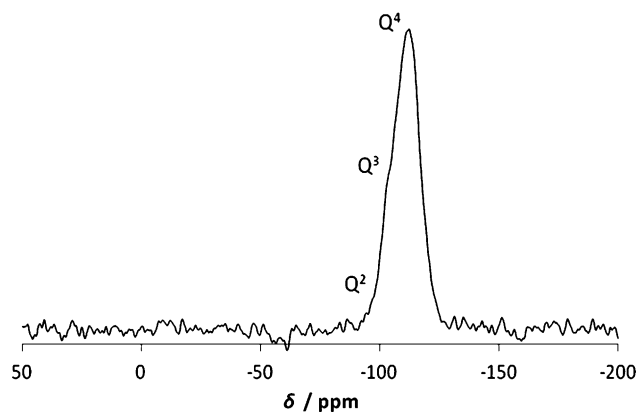


Figure 6.  $^{29}\text{Si}$  MAS NMR spectrum of material K13.

shape. However, the aggregates were of a similar diameter of approximately  $5\ \mu\text{m}$ . TEM images of all materials demonstrated a clear arrangement of the porous material with a uniform size. Figure 7a (SEM) and b (TEM) shows the micrographs of K13.

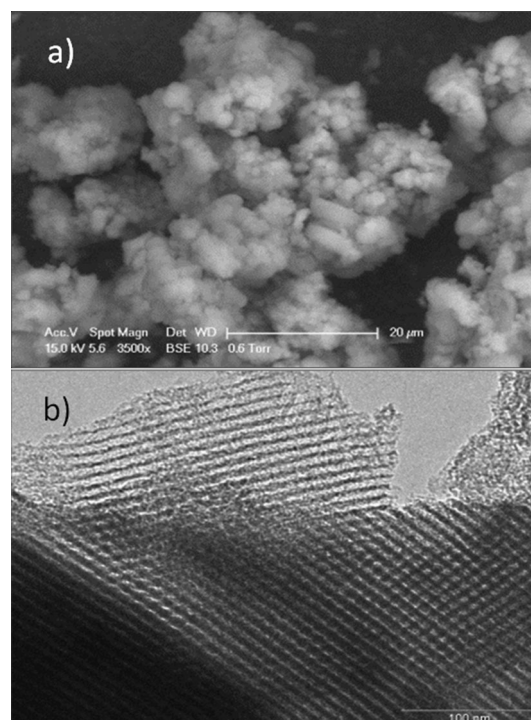


Figure 7. a) SEM and b) TEM micrographs of K13.

## In vitro studies

### Compounds and materials with an in vitro anti-proliferative effect against human cells

The capacity of the newly synthesised titanocene compounds to inhibit human cell proliferation in vitro was studied by evaluating their cytotoxicity on three human tumour cell lines: A2780 ovary carcinoma, MCF-7 breast adenocarcinoma and DLD-1 colon carcinoma. To establish their selectivity, the toxicity of the titanocene derivatives to HEK-293 human normal embryonic kidney cells was also tested.

Anti-proliferative activity was quantified by using  $\text{IC}_{50}$  values. The  $\text{IC}_{50}$  value is the concentration necessary to reduce the cell population's growth by 50%. Consequently, large  $\text{IC}_{50}$  values indicate nontoxic compounds and a decrease in the  $\text{IC}_{50}$  value indicates anti-proliferative behaviour. For 11–20, these parameters were calculated from the dose-response sigmoid curves provided by the GraphPad Prism biostatistics program. The studied compounds exhibit different grades of toxicity against the tested cell lines (Figure 8 and Table 4). Most of them are less toxic against the normal cell line (HEK-293) than to the human cancer cell lines. In particular, A2780 cells and MCF-7 cells were more affected by the titanocene complexes, which indicated some degree of selectivity of these compounds against the studied cancer cell lines.

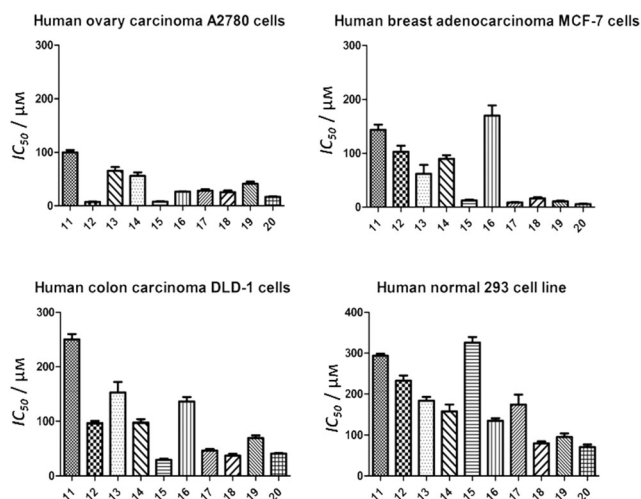


**Figure 8.** Histograms showing the  $IC_{50}$  values in  $\mu\text{M}$  for **11–20** and  $M_{50}$  in  $\mu\text{g mL}^{-1}$  for **KIT-6** and **K11–K20** on A2780, MCF-7, DLD-1 and HEK-293 at 24 h of action.

**Table 4.** Cytotoxicity values ( $IC_{50}$  in  $\mu\text{M}$  for **11–20** and  $M_{50}$  in  $\mu\text{g mL}^{-1}$  for **KIT-6** and **K11–K20**) on A2780, MCF-7, DLD-1 and HEK-293 at 24 h of action.<sup>[a]</sup>

	$IC_{50}$ [ $\mu\text{M} \pm \text{SD}$ ]/ $M_{50}$ values [ $\mu\text{g mL}^{-1} \pm \text{SD}$ ]			
	A2780	MCF-7	DLD-1	HEK-293
<b>11</b>	100.07 ± 7.85	143.80 ± 16.39	250.32 ± 17.20	293.90 ± 8.42
<b>12</b>	7.49 ± 1.06	103.13 ± 19.42	96.67 ± 6.89	232.67 ± 21.75
<b>13</b>	65.67 ± 12.25	62.15 ± 28.40	152.75 ± 33.48	183.70 ± 15.76
<b>14</b>	56.23 ± 11.20	90.19 ± 10.95	97.65 ± 10.45	157.41 ± 28.98
<b>15</b>	7.83 ± 1.54	12.55 ± 2.79	29.67 ± 3.55	326.50 ± 23.22
<b>16</b>	26.57 ± 1.12	170.33 ± 32.61	136.33 ± 13.97	134.43 ± 10.86
<b>17</b>	28.46 ± 4.66	8.84 ± 1.09	46.60 ± 5.11	174.30 ± 41.78
<b>18</b>	25.72 ± 5.47	16.45 ± 3.64	37.44 ± 5.65	79.92 ± 8.49
<b>19</b>	41.42 ± 6.86	10.80 ± 2.44	69.62 ± 8.54	95.39 ± 15.20
<b>20</b>	16.91 ± 1.66	5.92 ± 1.00	41.06 ± 1.94	70.77 ± 10.96
<b>KIT-6</b>	2404 ± 323	> 2500	2212 ± 204	> 2500
<b>K11</b>	1281 ± 156	1971 ± 120	2057 ± 136	717 ± 102
<b>K12</b>	193 ± 29	2040 ± 242	446 ± 38	1081 ± 214
<b>K13</b>	766 ± 152	857 ± 62	1834 ± 138	1086 ± 172
<b>K14</b>	299 ± 58	486 ± 67	504 ± 57	445 ± 48
<b>K15</b>	111 ± 18	163 ± 24	236 ± 31	1762 ± 183
<b>K16</b>	225 ± 34	1260 ± 131	840 ± 59	590 ± 148
<b>K17</b>	996 ± 92	278 ± 25	1079 ± 86	1254 ± 216
<b>K18</b>	489 ± 24	450 ± 70	714 ± 27	704 ± 104
<b>K19</b>	424 ± 50	124 ± 11	508 ± 46	650 ± 47
<b>K20</b>	85 ± 12	36 ± 5	149 ± 27	256 ± 42

[a] SD = standard deviation.

For the A2780 cell line, compounds **11**, **13**, **14** and **19** showed the highest  $IC_{50}$  values (from ca. 41 to 100  $\mu\text{M}$ ), whereas **16**, **17** and **18** were slightly more cytotoxic ( $IC_{50}$  values of ca. 26  $\mu\text{M}$ ). However, compounds **12**, **15** and **20** showed the highest cytotoxic activities against this cancer cell line with  $IC_{50}$  values from (7.49 ± 1.06) to (16.91 ± 1.66)  $\mu\text{M}$ . The cytotoxicity of the last compounds is much higher than that of titanocene dichloride in this cell line.<sup>[48]</sup> In addition, the cytotoxic activity of **12**, **15**, **16** and **20** is also higher than that reported for other active titanocene compounds with alkyl or arylammonium sub-

stituents at the Cp ring,<sup>[49–52]</sup> which are considered to be highly cytotoxic, comparable to titanium(IV)–salen complexes<sup>[53]</sup> and mixed titanocene–gold(I) derivatives.<sup>[54]</sup>

On the other hand, in human breast carcinoma (MCF-7 cells), the differences are more pronounced between the group of the less cytotoxic compounds formed by **11**, **12**, **13**, **14** and **16** (with  $IC_{50}$  values from ca. 60 to 170  $\mu\text{M}$ ) versus the more cytotoxic **15**, **17**, **18**, **19** and **20** (with  $IC_{50}$  values from ca. 5 to 17  $\mu\text{M}$ ). For the last five compounds, the  $IC_{50}$  values display a significant drop in comparison with the rest of the titanocenes (one-way ANOVA test, Bonferroni post-test,  $p < 0.05$ ). The most cytotoxic compounds of the series reported herein present higher cytotoxicity than other titanocene derivatives<sup>[55–58]</sup> and comparable cytotoxicity in this cell line with the famous and highly cytotoxic compound titanocene-Y reported by Tacke and co-workers.<sup>[59,60]</sup>

Proliferation of the aggressive K-ras mutant DLD-1 colon cells was also reduced by using the titanocene compounds **11–20**. For this cell line  $IC_{50}$  values were somewhat larger compared with the other two cell lines. Compounds **15**, **17**, **18** and **20** maintained their relatively high cytotoxicity against DLD-1 cells, although with higher  $IC_{50}$  values than those in the other cell lines (from ca. 30 to 47  $\mu\text{M}$ , which are the lowest  $IC_{50}$  values described in the literature for DLD-1 cells). The remaining titanocene derivatives **11–14**, **16** and **19** showed relatively low cytotoxic activity against DLD-1 with  $IC_{50}$  values ranging from about 70 to 250  $\mu\text{M}$ .

A correlation between the toxicity of the compounds (nonparametric Spearman two-tailed correlation, non-significant  $p$  value summary  $r > 0.3$ ,  $p > 0.2$ ) and the different cell types was not found.

Analysis of the toxicity of **11–20** towards normal cell lines (HEK-293) shows, in general, much higher  $IC_{50}$  values (lower toxicity) for all complexes in comparison with the  $IC_{50}$  values obtained for cancer cell lines. In particular, compounds **15** and **20** show a very high degree of selectivity (much greater than that observed for the other compounds). This is due to the ability of **15** and **20** to strongly inhibit the three studied tumour cell lines, which results in  $IC_{50}$  value ratios between tumoural and normal cells superior to those of the other compounds (for further information, see Table S1 in the Supporting Information).

Additionally, the anti-proliferative activity of the titanocene-functionalised materials **K11–K20** and the unmodified mesoporous material **KIT-6** was tested against cancer cell lines A2780, MCF-7, DLD-1 and normal cells HEK-293. The  $M_{50}$  values (which is the concentration of material necessary to reduce the cell population's growth by 50%) were determined and are given in Table 4 and Figure 9.

The non-functionalised mesoporous matrix **KIT-6** does not show any significant activity against the studied cell lines, whereas materials **K11–K20** exhibited, in general, high cytotoxic activity against cancer cell lines, but only moderate activity against normal cell line HEK-293.

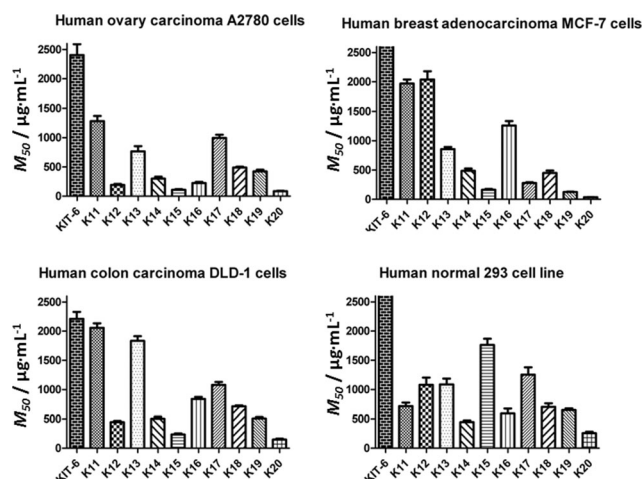


**Figure 9.** Histograms showing the  $M_{50}$  values in  $\mu\text{g mL}^{-1}$  for K11–K20 on A2780, MCF-7, DLD-1 and HEK-293 at 24 h of action.

In particular, materials **K11**, **K13**, **K16** and **K17** display lower toxicity in tumour cell lines than **K15**, which exhibits a statistically significant anti-proliferative effect against the three tumour cell lines. Furthermore, material **K12** shows a high cytotoxic effect against ovary and colon carcinoma cells and **K18** against ovary and breast tumoural cells (one-way ANOVA test, Dunnet post-test, 95% confidence interval), but their selectivity is low because the  $M_{50}$  values against the normal cell line HEK-293 are in the same concentration range.

Again, as in the case of the titanocene derivatives **15** and **20**, materials **K15** and **K20** are the most potent cytotoxic agents in all the three tumour cell populations, with a pronounced statistical significance (Bonferroni post-test,  $p < 0.001$ ). This confirms the fact that these titanocene structures give the best activity for the studied compounds. The proportion between the titanocene  $IC_{50}$  and material  $M_{50}$  values is maintained in all tumour cell lines. In A2780 cells, the correlation is significant (nonparametric correlation between two data sets, Spearman  $r$  value of 0.7697, two-tailed  $p$  value of 0.0126); the same is observed in DLD-1 cells ( $r = 0.66$ ,  $p = 0.0438$ ). However, in MCF-7 cells, the association is even more pronounced ( $r = 0.90$ ,  $p = 0.0008$ ). For example, ratios of  $11.67 \pm 3.06$  in **K15/15** activity, and  $4.90 \pm 1.23$  in **K20/20** activity in tumour cell lines are observed. For this reason, material **K15** appears to have a higher selectivity than **K20** when compared with the  $M_{50}$  value of the studied normal cell line. This phenomenon occurs even if there is no correlation between the absolute values of titanocene toxicity versus material toxicity for most of the compounds, mainly because the relative proportion of titanocene is not identical in all nanostructured materials. Therefore, we have calculated the cytotoxic activity of all of the functionalised materials in terms of Ti  $M_{50}$  index (which represents the quantity of anchored titanium needed to inhibit normal cell growth by 50%; Table 5). The results show a similar tendency to that found for the  $M_{50}$  values; materials **K15** and **K20** are the most cytotoxic compounds for the three cancer cell lines and present moderate toxicity to the HEK-293 cells,

**Table 5.** Cytotoxicity values (Ti  $M_{50}$  in  $\mu\text{g mL}^{-1}$  of Ti anchored on the surface) on A2780, MCF-7, DLD-1 and HEK-293 of the titanocene-functionalised materials **K11**–**K20** at 24 h of action.

Material	Ti $M_{50}$ values ( $\mu\text{g mL}^{-1} \pm \text{SD}$ )			
	A2780	MCF-7	DLD-1	HEK-293
<b>K11</b>	$27.3 \pm 3.3$	$42.0 \pm 2.6$	$43.8 \pm 2.9$	$15.3 \pm 2.2$
<b>K12</b>	$2.3 \pm 0.3$	$24.5 \pm 2.9$	$5.4 \pm 0.5$	$13.0 \pm 2.6$
<b>K13</b>	$16.6 \pm 3.3$	$18.6 \pm 1.3$	$39.8 \pm 3.0$	$23.6 \pm 3.7$
<b>K14</b>	$6.8 \pm 1.3$	$11.0 \pm 1.5$	$11.4 \pm 1.3$	$10.1 \pm 1.1$
<b>K15</b>	$3.4 \pm 0.6$	$5.0 \pm 0.7$	$7.2 \pm 0.9$	$53.9 \pm 5.6$
<b>K16</b>	$5.5 \pm 0.8$	$30.6 \pm 3.2$	$20.4 \pm 1.4$	$14.3 \pm 3.6$
<b>K17</b>	$22.2 \pm 2.1$	$6.2 \pm 0.6$	$24.1 \pm 1.9$	$28.0 \pm 4.8$
<b>K18</b>	$9.8 \pm 0.5$	$9.0 \pm 1.4$	$14.3 \pm 0.5$	$14.1 \pm 2.1$
<b>K19</b>	$10.3 \pm 1.2$	$3.0 \pm 0.3$	$12.3 \pm 1.1$	$15.8 \pm 1.1$
<b>K20</b>	$4.1 \pm 0.6$	$1.7 \pm 0.2$	$7.2 \pm 1.3$	$12.4 \pm 2.0$

and show again remarkable selectivity towards cancer cell lines (for further information, see Table S2 in the Supporting Information).

In general, the materials reported herein, especially **K15** and **K20**, present much higher cytotoxic activity (lower  $M_{50}$  or Ti  $M_{50}$  values) and selectivity than other similar nanostructured systems functionalised with titanocene derivatives reported by us.<sup>[33–36]</sup>

Due to their superior cytotoxic properties in terms of activity and selectivity, **15**, **20**, **K15** and **K20** were selected to study the cell death mechanisms and signalling pathway interferences (see the section on apoptotic studies).

#### Apoptosis induction capacity of titanocene complexes and titanocene-functionalised mesoporous materials

To establish the type of damage induced by the novel synthesised compounds, the mechanism of cell death was analysed by flow cytometric methods. The behaviour of compounds **15** and **20**, along with their analogous nanomaterials (**K15** and **K20**), was analysed in A2780 ovary carcinoma, MCF-7 breast adenocarcinoma and DLD-1 colon carcinoma cell lines.

For these studies, the fluorescein isothiocyanate (FITC) stained, AnnexinV marked cells corresponded to the early apoptotic stages, whereas double colouration indicated a distinct population in early/mid apoptotic stages in which the translocation of membrane proteins was added to DNA fragmentation and loss of nuclear DNA content, marked by propidium iodide (PI) fluorochrom, which was capable of binding and labelling DNA (Figure 10).<sup>[61]</sup> PI colouration only indicates late apoptosis; the magnitude of the PI-marked DNA damage in the context of cell cycle arrest is also reflected (Figure 11).

For A2780 ovary cells, a strong anti-proliferative activity of complex **15** was confirmed and in all compounds the shift to the mid and late stages of apoptosis was observed within 8 h. Translation to the late stages of apoptosis with DNA damage is more pronounced for **K15** and **K20** materials (for further details, see Figure S8 in the Supporting Information). Regarding MCF-7 breast carcinoma, all studied compounds and materials had a better capacity to induce apoptosis, in comparison with the standard chemotherapy drug oxaliplatin. The apoptotic ac-

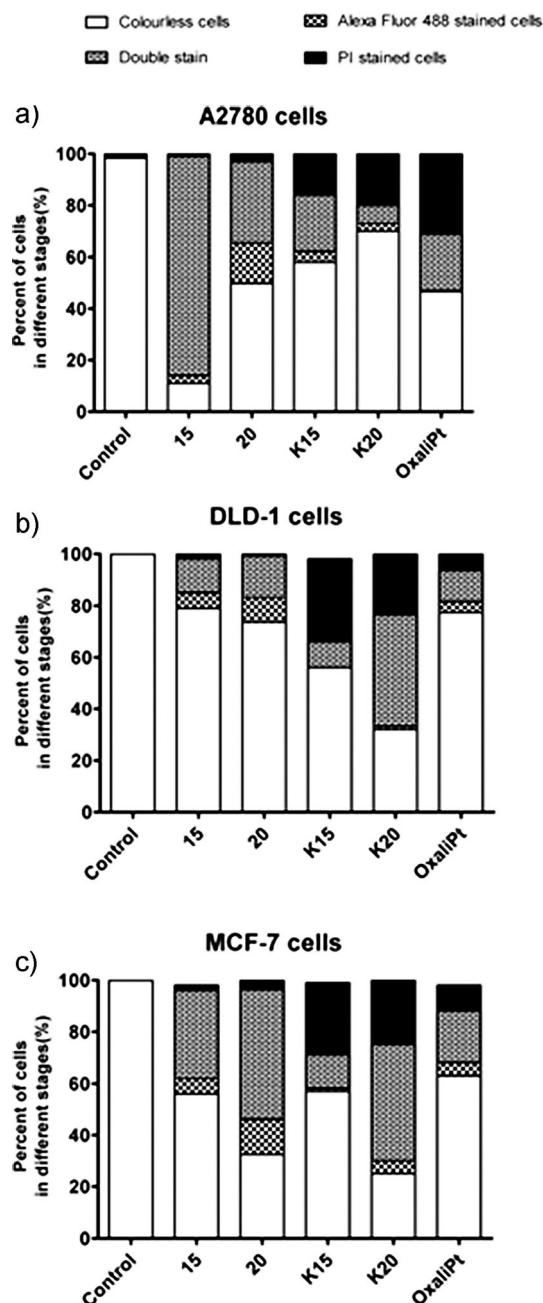


**Figure 10.** Apoptosis induction by titanocene derivatives in a) A2780, b) MCF-7 and c) DLD-1 cancer cells. Flow cytometry provides data about the resulting cell populations after 8 h of treatment with titanocene compounds 15 and 20 and nanostructured materials K15 and K20; colourless cells are living cells, and the rest of the cells are non-viable and divided into three different populations with specific attributes of cell death.

tivity of K15 and K20 was comparable or superior to that of the analogous titanocene complexes. In addition, the proportion of cells in mid- and late-stage apoptosis was superior to that of the “free” titanocene derivatives 15 and 20 (Figure 11). In DLD-1 cells, treatment with the titanocene-functionalised nanostructures not only conveyed cell death, but also accelerated the transition of cells to late apoptotic stages and induced massive DNA damage (for further details, see Figure S9 in the Supporting Information).

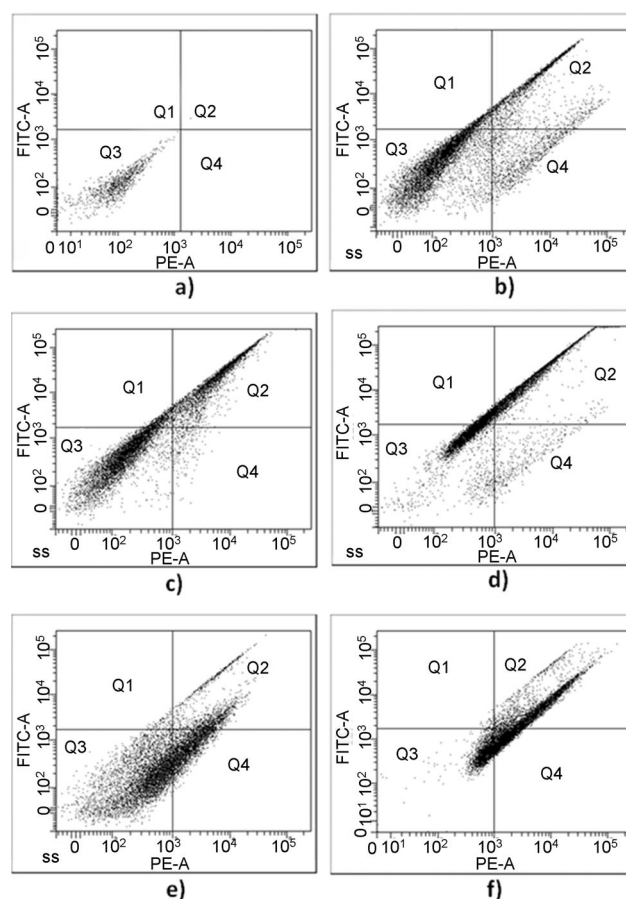


**Figure 11.** Flow cytometric evaluation of apoptosis induction by titanocenes and nanostructured materials: a) untreated control MCF-7 cells, b) oxaliplatin-treated cells, c) cells treated with 15, d) cells treated with 20, e) cells treated with K15, f) cells treated with K20. Viable cells are found in the Q3 box, the Q1 box corresponds to FITC-labelled early apoptosis cells, double colouration is located in the Q2 quadrant, and in Q4 PI indicates late apoptosis.

In general, despite the very low quantity of titanium in functionalised materials K15 and K20, compared with that of the “free” titanocene derivatives, the materials present a higher apoptotic activity, which indicates that the grafting of titanocene derivatives on silica-based mesoporous materials has a positive influence on the cytotoxic properties of the titanocene complexes.

Mounting evidence in the literature shows that tumour cell evasion of programmed cell death is critical for cancer progress and unremitting growth and the success of a chemotherapeutic drug is dependent on its capacity to promote apoptosis.<sup>[62]</sup> Therefore, not only the toxicity, but the apoptosis inducing capacity of the compounds are important issues associated with the analysed agents, especially for K15 and K20.

#### Evaluation of the modulator effect on the intrinsic apoptotic pathway

We have measured the expression of two antagonist proteins, members of the Bcl-2 family, which have a very important function in the intrinsic apoptotic pathway. The Bax- $\alpha$  proapop-

otic and Bcl-xL anti-apoptotic molecule expressions vary between different cells lines because they are tumours derived from different organs. This observation is supported by numerous reports in the literature.<sup>[62-67]</sup>

In A2780 cells, treatment with **15** shows evident Bax- $\alpha$  overexpression, whereas in the other cases the molecule is suppressed (Figure 12). In MCF-7 breast carcinoma cells, **15**, **20** and **K20** lead to proapoptotic Bax- $\alpha$  upregulation in a statistically relevant proportion; the concentration of the molecule is much higher than that observed upon treatment with oxaliplatin (Figure 12). In colorectal carcinoma DLD-1, Bax- $\alpha$  expression is prominent for **K15**; for **K20**, suppression is less than that provoked by oxaliplatin (all data compared with column statistics, one-way analysis of variance,  $p < 0.001$ ; Figure 12).

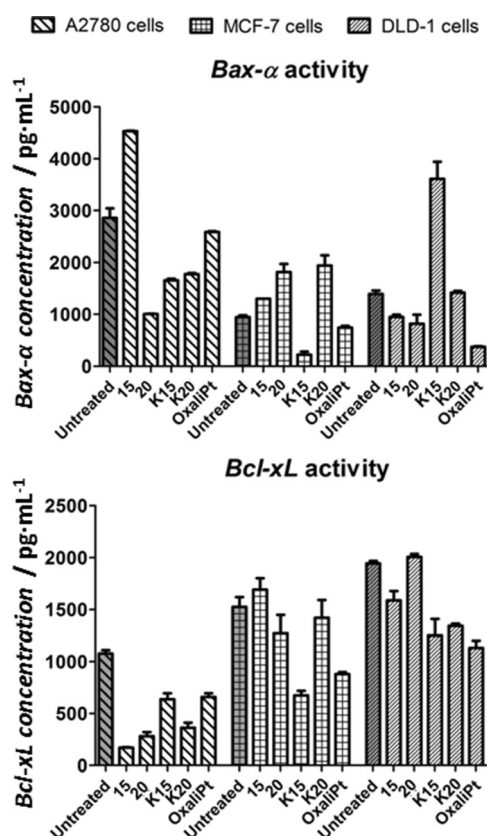


**Figure 12.** Modulation of Bax- $\alpha$  expression in untreated malignant cells and malignant cells treated with oxaliplatin, **15**, **20**, **K15** and **K20** (top). Modulation of Bcl-xL expression in untreated malignant cells and malignant cells treated with oxaliplatin, **15**, **20**, **K15** and **K20** (bottom).

The anti-apoptotic Bcl-xL protein expression is downregulated in A2780 cells for the studied compounds and materials: **15** is strongly suppressed and for **20** and **K20** downregulation is more important than that caused by the platinum drug (Figure 12). In MCF-7 cells, material **K15** exhibits the most important suppression (higher than that caused by oxaliplatin), whereas in DLD-1 cells **15**, **K15** and **K20** downregulate the anti-apoptotic molecule similarly to oxaliplatin (all data analysed by column statistics, two-tailed ANOVA test, Bonferroni post-test,  $p = 0.001$ ).

Bearing in mind that the Bax- $\alpha$ /Bcl-xL ratio is a mathematical parameter with relevance for promotion of the apoptotic process, we can infer that when this ratio is higher than one, apoptotic cell death is induced and when this ratio is much lower than one and close to zero the cell is resistant to apoptotic stimuli.<sup>[64]</sup> For **K15** and **K20**, this ratio is higher than one in all the cell lines, with a single exception (material **K15** in MCF-7 breast cancer), and is much higher in comparison with the untreated cell basal value. Thus, in A2780, the ratios are 4.897 for **K20**, 2.596 for **K15**; 1.366 for **K20** in MCF-7 cells, and 1.056 for **K20** and 2.887 for **K15** in DLD-1 cells. The Bax- $\alpha$ /Bcl-xL ratio induced by the materials is superior to the ratio corresponding to the titanocene compounds in DLD-1 cells, for which the ratio is 0.407 for **20** and 0.598 for **15**. The same trend is observed for titanocene **20** in the cell lines MCF-7 (ratio value 1.074) and A2780 (ratio value 3.58). In both cases, the "free" titanocene action is inferior to that of the analogous materials. This tendency is not followed by **K15** in A2780 cells, for which its ratio is lower than that observed for **15**. Although both **K15** and **K20** induce a large amount of apoptotic events, the intrinsic pathway seems to be triggered more efficiently by **K20**, whereas **K15** appears to take other pathways.

Apoptotic cell death is regulated by complex interactions between pro-survival members and two subgroups of pro-apoptotic members of the B-cell lymphoma-2 (Bcl-2) protein family. In the intrinsic apoptotic pathway, two crucial cell death switch molecules have important regulatory functions: Bax- $\alpha$  and Bcl-xL. The Bax- $\alpha$  protein promotes the apoptotic processes, for which caspases activation is involved, whereas anti-apoptotic Bcl-xL, which is a protein located in the mitochondrial membrane, acts in the direction of cell survival by blocking the apoptotic signals.<sup>[63]</sup> The two molecule expression is used as a molecular marker in tumours and has an important prognostic value in cancer diagnostics and chemotherapy follow up.<sup>[68]</sup> Modern molecular therapies use innovative drugs to reach these molecular targets in breast cancer,<sup>[69]</sup> ovarian carcinoma, and other malignant diseases;<sup>[70]</sup> consequently the capacity of **K15** and **K20** to modulate production of the two proteins is very important in defining their biological potential, and thus, their possible application in chemotherapy.

#### Apoptosis regulation at the DNA level: Inhibition of PARP-1

When cells are exposed to external factors, such as apoptosis trigger molecules or drugs, and DNA damage occurs, cellular stress responses are determined by specific regulatory processes. In the nucleus, the poly(ADP-ribose) polymerase-1 enzyme (PARP-1) functions at the centre of cellular stress responses and facilitates DNA repair by catalysing the ADP-ribosylation of proteins.<sup>[71]</sup> This is why PARP-1 is a target for anti-cancer drugs, and its inhibition may be a way to enhance the apoptotic signalling pathways in tumour cells. The capacity of **15**, **20**, **K15** and **K20** to cleave PARP-1 was assessed after incubation of a histone-coated plate with different dilutions of the compounds/materials of interest for 1 h.

All analysed agents display moderate PARP-1 inhibitory activity, below that of the reference compound, 3-aminobenz-

amide (Figure 13). The maximum PARP-1 inhibitory activity is above the  $IC_{50}$  concentration, especially for the titanocenes. Thus, the activity of **K15** and **K20** is somewhat better than that of **15** and **20**. By taking into account that there is a reduced amount of active titanocene compounds in the mesoporous materials, a plausible conclusion is that the titanocene compounds anchored onto nanostructured materials are more efficient than the "free" titanocene derivatives in counteracting DNA damage repair.

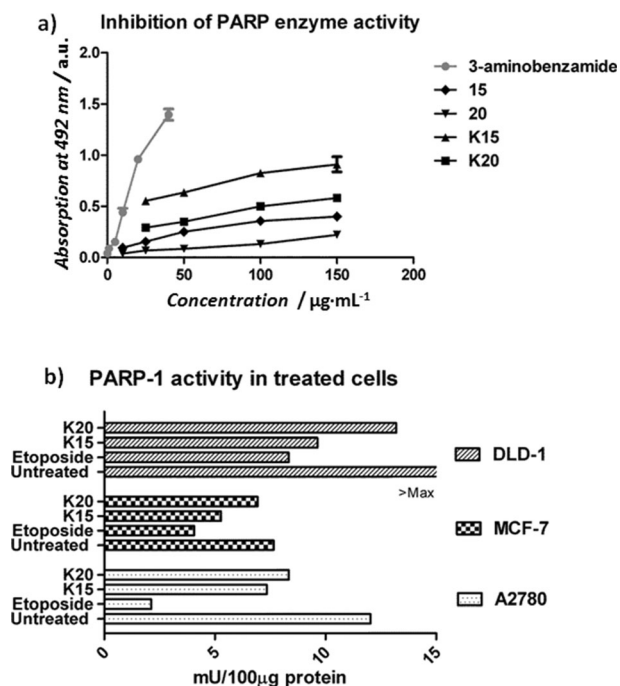


**Figure 13.** a) Capacity of etoposide, **15**, **20**, **K15** and **K20** to inhibit the PARP-1 enzyme and counteract DNA damage repair and b) DNA damage caused by treatment with etoposide, **15**, **20**, **K15** and **K20** quantified by the decrease of PARP-1 activity. In the treated malignant cells, the PARP-1 activity decreases due to cleavage of the molecule during apoptosis.

In this context, DNA damage caused by titanocene-functionalised nanostructured materials **K15** and **K20** was quantified by the magnitude of PARP-1 cleavage. The PARP-1 activity was evaluated in material-treated cell lysates to establish the amount of fragmented PARP-1. Etoposide is a recognised apoptosis inducer drug and it was used as a reference compound provided by the PARP-1 measuring kit.

In the A2780 cell population, the PARP-1 molecule is strongly expressed and it has been reported that is cleaved by apoptosis-inducing drugs, such as platinum drugs.<sup>[72]</sup> The analysed materials **K15** and **K20** are also able to cleave PARP-1, but their capacity is below the standard etoposide. In DLD-1 cells, where PARP-1 is also overexpressed (higher levels outside the limits of our assessment), the two nanostructured materials **K15** and **K20** cause a higher level of DNA damage in the cells, although the PARP-1 activity is decreased compared with the etoposide treatment. However, this is an important aspect because standard drugs, such as cisplatin, are unable to cleave this enzyme in DLD-1 cells.<sup>[73]</sup> The results in MCF-7 cells show

that the expression is weaker compared with that of the other tumour cells, and a reduction in the PARP-1 activity caused by **K20** and **K15** is observed.

Bearing in mind that PARP-1 is implicated in the Fas-induced extrinsic apoptosis pathway, in the caspases cascade, in tumour growth factor  $\beta$  (TGF- $\beta$ ) receptor signalling and is of utmost importance in cancer cell growth regulation, its cleavage provides evidence of DNA damage caused by the titanocene-functionalised materials **K15** and **K20**. Thus, in breast carcinoma, data in the literature show that there is a significant correlation between PARP expression and members of the Bcl-2 family.<sup>[69]</sup> In MCF-7 breast cancer cells,<sup>[71]</sup> PARP-1 cleavage by caspase-3 is an important step in the apoptotic signal pathway, although, even in the absence of caspase-3, Bax- $\alpha$  overexpression induces DNA fragmentation and apoptosis. On the other hand, apoptotic events occur in treated DLD-1 cells<sup>[73]</sup> by PARP fragmentation from its 113 kDa intact form to a 85 kDa cleaved protein, following metal-based drug action. In addition, after certain treatments, the 82 kDa band can appear, which is detected by the anti-cleaved PARP (Asp214) antibody available.

Thus, PARP-1 can recognise DNA lesions caused by platinum-based drugs through PARP-1 binding to the damaged intrastrand cross-links.<sup>[74]</sup> Titanocene compounds are also capable of causing DNA damage,<sup>[50]</sup> and we expect a similar interaction with PARP-1 and the material-damaged DNA.

The interconnections between phosphatidylserine translocation, Bax- $\alpha$  and Bcl-xL expression, and the PARP enzyme activity may be one reason why a decrease in PARP-1 cleavage and DNA repair is observed for the three cell lines studied, even though the compounds themselves are modest enzyme inhibitors.

In **15** or **K15** action against tumour cells, for which proapoptotic Bax- $\alpha$  is overexpressed, significant poly-ADP-ribose cleavage was recorded, despite the weak PARP-1 inhibitory capacity of the compounds.

#### Titanium release and cellular uptake

In view of the interesting results obtained in all biological experiments associated with **15**, **20**, **K15** and **K20**, we decided to explore the titanium uptake of the treated cells in an attempt to correlate this with the cytotoxicity and other effects observed previously. The first question that we had to try to answer was whether there were some differences in the quantities and/or way of titanium uptake by cells treated with the titanium derivatives (**15** and **20**) or with the titanium-functionalised materials (**K15** and **K20**). Thus, cells were treated with the studied compounds or materials at concentrations of 500  $\mu\text{M}$  (**15** and **20**) and 500  $\mu\text{g}\cdot\text{mL}^{-1}$  (**K15** and **K20**); the final concentration of Ti in the cell culture media was 23.91  $\mu\text{g}\cdot\text{mL}^{-1}$  for **15**, 23.90  $\mu\text{g}\cdot\text{mL}^{-1}$  for **20**, and, according to the Ti-functionalisation rates, 15.3  $\mu\text{g}\cdot\text{mL}^{-1}$  in **K15** and 24.25  $\mu\text{g}\cdot\text{mL}^{-1}$  in **K20**.

After 24 h of treatment, surprisingly, the quantity of titanium in populations of  $10^6$  cells was higher in the case of titanium-functionalised materials (**K15** and **K20**); incorporation ranging from about 4 to 23% of the total amount of titanium was observed, whereas **15** and **20** showed incorporation that ranged

**Table 6.** Titanium concentration in a population of  $10^6$  treated cancer cells and titanium incorporation efficiency calculated as titanium incorporated in  $10^6$  cells relative to the amount of titanium in the cell culture media.

	A2780 Ti [ $\mu\text{g}$ per $10^6$ cells]	A2780 Ti incorporation rate [%]	MCF-7 Ti [ $\mu\text{g}$ per $10^6$ cells]	MCF-7 Ti incorporation rate [%]	DLD-1Ti [ $\mu\text{g}$ per $10^6$ cells]	DLD-1 Ti incorporation rate [%]
<b>15</b>	$110 \pm 2$	4.6	$9 \pm 0.2$	0.4	$14 \pm 0.2$	0.6
<b>20</b>	$57 \pm 1$	2.4	$25 \pm 1$	1.0	$10 \pm 0.4$	0.4
<b>K15</b>	$165 \pm 0.2$	10.8	$352 \pm 4$	23.0	$168 \pm 1.4$	11.0
<b>K20</b>	$248 \pm 2$	10.2	$460 \pm 2$	19.0	$114 \pm 4$	4.7

from about 0.4 to 4.6% titanium (Table 6; for further details, see Tables S3–S5 in the Supporting Information). These results indicate an interesting property of the titanium-functionalised materials, which appear to be acting as a Trojan horse for the incorporation of the titanium active species into the cells. This leads to much higher quantities of titanium uptake in cells, probably because permeation or adherence of the materials to the cells is relatively high. What is clear from these experiments is that the transport processes (either active or passive) of “free” titanocene derivatives to the cell are less effective than in the case of titanocene-functionalised materials; this may be due to the tendency towards hydrolysis and/or decomposition of titanocene compounds in physiological medium, which leads to a decrease in the cytotoxicity due to the impossibility of titanium reaching the cell. It seems, therefore, that the most important steps associated with the *in vitro* properties of these compounds are the transport of active species to the cell.

In addition, from the data obtained in the uptake experiments, we were able to correlate the titanium uptake with some other properties discussed previously. Thus, in cancer cells treated with materials **K15** and **K20**, the Ti incorporation rate is significantly correlated with the cytotoxicity, expressed as  $M_{50}$  values (two-tailed correlation, Pearson  $r=0.8925$  in the 95% confidence interval,  $p=0.0167$ ;  $R^2=0.966$ ), whereas in compounds **15** and **20** no such association was found.

However, the cellular uptake in cells treated with **15** and **20** is related to the number of apoptotic cells in the treated population (the sum of early and late apoptotic cells, those with Alexa Fluor stain and double PI/Alexa Fluor stain; Pearson  $r$  value = 0.8315, significant  $p=0.0402$ , and  $R^2=0.6914$ ). Additionally, cellular inclusion of the compounds correlates significantly with the Bax- $\alpha$  expression (two-tailed correlation, Pearson  $r$  value 0.8267 in the 95% confidence interval,  $p=0.0425$ ;  $R^2=0.6834$ ). The Ti incorporation efficiency is also strongly related with Bax- $\alpha$  expression ( $r=0.8755$ ,  $p=0.0223$ ;  $R^2=0.7665$ ). Furthermore, Ti uptake is related with Bcl-xL expression when tumour cells are treated with **15** and **20**, showing a negative correlation with the anti-apoptotic molecule, ( $r=-0.8597$ ,  $p=0.0281$ , 0.7392). The Ti incorporation rate is also negatively connected to Bcl-xL with statistical significance ( $r=-0.9133$ ,  $p=0.0109$ ,  $R^2=0.8341$ ).

On the other hand, in tumour cells treated with materials **K15** and **K20**, Ti uptake can be significantly correlated with the PARP value (Pearson  $r=0.9289$  in the 95% confidence interval, two-tailed  $p$  value = 0.0074,  $R^2=0.8629$ ).

Thus, we have determined that the titanium uptake data indicate that the Ti cellular uptake amount delineates the capacity of **15** and **20** to trigger apoptosis, whereas in the case of the materials the Ti uptake amount is correlated with their cytotoxicity and PARP cleavage.

To be certain that this high quantity of titanium uptake in cells treated with materials **K15** and **K20** is due to protection of the titanium compounds by the mesoporous system KIT-6, release studies were performed. Thus, taking into account that the titanocene compounds supported on the KIT-6 matrix are normally bound to the material through Ti–O–Si bonds and that these are normally stable in aqueous solutions at physiological pH (as previously observed by our group),<sup>[33–36]</sup> no release, or a very low amount, of titanium-containing water-soluble species is expected for these materials. In this context, suspensions of materials **K15** and **K20** in simulated body fluid were incubated at 37 °C in a water bath for 72 h and the suspensions subsequently filtered. When the filtrate was analysed by inductively coupled plasma atomic emission spectroscopy (ICP-AES), a very low titanium amount (lower than the 0.01% of the titanium in each material) was observed, which indicated that no release of the titanocene derivative occurred in these experiments.

The lack of release of titanium-soluble species confirms that the cytotoxic properties of the corresponding titanocene-functionalised materials is probably due to particle action and not to the release of the corresponding titanocene compound or some other titanium-containing active species. These results show again that the mesoporous silica-based material therefore promotes higher titanium uptake by the cells.

It also seems plausible that the different  $\text{TiCp}_2$  moieties attached to the surfaces, together with the titanium content of the material, may have a real influence on the cytotoxicity and that is why different materials with similar titanium contents, but different supported compounds have completely different cytotoxic properties. Therefore, the release of the titanocene compound does not seem to be necessary for cytotoxicity. However, functionalisation of materials with titanocene is crucial because non-functionalised KIT-6 does not present cytotoxic properties.

## Conclusion

A series of alkenyl-substituted titanocene compounds have been synthesised and characterised. These compounds have been subsequently grafted onto a nanostructured silica-based

porous material, KIT-6, to give titanocene-functionalised materials, which have been synthesised and characterised by various techniques. It has been observed that the titanocene derivatives are normally bound, through  $\mu$ -oxo surface species, to the external surface of the mesoporous matrix.

All of the synthesised compounds and materials have been tested in vitro against different human cancer cell lines and a normal human cell line. A very high activity of the studied titanocene derivatives has been observed and is much higher than the majority of the titanocene derivatives reported in the literature, and comparable to that of famous titanocene-Y, which is one of the most potent metallodrugs based on titanium.

In addition, the titanocene-functionalised materials reported herein, present much higher cytotoxic activity (lower  $M_{50}$  or  $Ti M_{50}$  values) and selectivity than other similar nanostructured systems functionalised with titanocene derivatives.

From studies of the apoptosis induction capacity, evaluation of the modulator effect on the intrinsic apoptotic pathway, apoptosis regulation at the DNA level and titanium uptake by cells, one can conclude that the dynamics of apoptotic morphological and functional changes is modified when the active titanocenes are incorporated onto mesoporous materials. **15**, **20**, **K15** and **K20** are able to induce programmed cell death in tumour cell populations, by impairing the damaged DNA repair mechanisms and by up-regulation of intrinsic and extrinsic apoptotic signalling pathways. In addition, it seems that titanium-functionalised materials are acting as Trojan horses for the incorporation of the titanium active species into the cells, leading to much higher quantities of titanium uptake in cells, so that transport processes (either active or passive) of "free" titanocene derivatives to the cell are less effective than in the case of titanocene-functionalised materials.

Therefore, the functionalised nanostructured materials **K15** and **K20** are good candidates for targeted anti-cancer therapy, not only because of their interesting biological properties, which have been reported herein, but also because of the higher permeation of the membranes of cancer cells in comparison with healthy cells. This may be advantageous for the specific use of these materials in chemotherapy, especially against bone tumours due to the physical properties of silica-based materials.

## Experimental Section

### Synthesis of titanocene complexes

Complexes **11**,<sup>[44]</sup> **12**,<sup>[75]</sup> **13**,<sup>[75]</sup> **15**,<sup>[75]</sup> and **16**<sup>[75]</sup> were prepared according to synthetic protocols described by us previously.

**Synthesis of 14:** A solution of **4** (1.79 g, 7.79 mmol) in THF (50 mL) was added dropwise over 10 min to a solution of  $[TiCl_4(thf)_2]$  (1.30 g, 3.89 mmol) in THF (50 mL) at 0 °C. The reaction mixture was allowed to warm to room temperature and stirred for 2–3 h. The solvent was then removed in vacuo and a 9:1 mixture of toluene/hexane (50 mL) was added to the resulting solid. The suspension was filtered to remove LiCl and the filtrate was concentrated (20 mL) and cooled to –30 °C to give **14** as a red solid (1.39 g, 63%). <sup>1</sup>H NMR (400 MHz, CDCl<sub>3</sub>, 25 °C, for the mixture of isomers):

$\delta$  = 1.79, 1.80 (s, 6H each; CMePh), 1.80–2.00 (m, 8H; CH<sub>2</sub>CH<sub>2</sub>CH=CH<sub>2</sub>), 2.16 (m, 8H; CH<sub>2</sub>CH<sub>2</sub>CH=CH<sub>2</sub>), 4.91 (m, 8H; CH<sub>2</sub>CH<sub>2</sub>CH=CH<sub>2</sub>), 5.22, 5.60, 6.11, 6.15, 6.29, 6.43, 6.51, 6.68 (m, 2H each; C<sub>5</sub>H<sub>4</sub>), 5.73 ppm (m, 4H; CH<sub>2</sub>CH<sub>2</sub>CH=CH<sub>2</sub>); <sup>13</sup>C{<sup>1</sup>H} NMR (100 MHz, CDCl<sub>3</sub>, 25 °C, for the mixture of isomers):  $\delta$  = 23.3, 24.3 (CH<sub>2</sub>CH<sub>2</sub>CH=CH<sub>2</sub>), 28.8, 28.9 (CH<sub>2</sub>CH<sub>2</sub>CH=CH<sub>2</sub>), 41.2, 42.6 (CMePh), 44.4, 44.5 (CpC), 145.7, 145.8 (C<sub>5</sub>H<sub>4</sub>), 146.8, 147.0 (C<sub>6</sub>H<sub>5</sub>), 138.7, 138.8 ppm (CH<sub>2</sub>CH<sub>2</sub>CH=CH<sub>2</sub>); FTIR (KBr):  $\tilde{\nu}$  = 1636 (C=C), 2870, 2934 (C<sub>ar</sub>-H), 3060 cm<sup>-1</sup> (C<sub>ar</sub>-H); EI-MS:  $m/z$  (%): 529 (10) [ $M^+$ -Cl], 341 (15) [ $M^+$ -C<sub>5</sub>H<sub>4</sub>{CMePhCH<sub>2</sub>CH<sub>2</sub>CH=CH<sub>2</sub>}], 250 (13) [ $M^+$ -C<sub>5</sub>H<sub>4</sub>{CMePhCH<sub>2</sub>CH<sub>2</sub>CH=CH<sub>2</sub>}-CH<sub>2</sub>CH<sub>2</sub>CH=CH<sub>2</sub>-Cl-H], 185 (75) [ $M^+$ -C<sub>5</sub>H<sub>4</sub>{CMePhCH<sub>2</sub>CH<sub>2</sub>CH=CH<sub>2</sub>}-CMePhCH<sub>2</sub>CH<sub>2</sub>CH=CH<sub>2</sub>+3H], 143 (77) [CMePhCH<sub>2</sub>CH<sub>2</sub>CH<sub>2</sub>CH<sub>2</sub>CH=CH<sub>2</sub>+2H] 117 (96) [ $M^+$ -2C<sub>5</sub>H<sub>4</sub>{CMePhCH<sub>2</sub>CH<sub>2</sub>CH=CH<sub>2</sub>}], 105 (38) [CMePh<sup>+</sup>+H], 91 (100) [C<sub>7</sub>H<sub>7</sub><sup>+</sup>]; elemental analysis calcd (%) for C<sub>34</sub>H<sub>38</sub>Cl<sub>2</sub>Ti (565.44 g mol<sup>-1</sup>): C 72.22, H 6.77; found: C 72.61, H 6.63.

**Synthesis of 17:** This compound was synthesised by using the same procedure as that described for **14**, with **5** (20.00 mL, 0.75 g, 3.83 mmol, 0.19 M in THF) and  $[Ti(\eta^5-C_5H_5)Cl_3]$  (0.80 g, 3.65 mmol). Yield: 0.36 g, 26%; <sup>1</sup>H NMR (400 MHz, CDCl<sub>3</sub>, 25 °C):  $\delta$  = 1.34 (s, 6H; CpCMe<sub>2</sub>), 1.44, 1.65 (m, 2H each; CH<sub>2</sub>CH<sub>2</sub>CH=CMe<sub>2</sub>), 1.49, 1.63 (s, 3H each; CH<sub>2</sub>CH<sub>2</sub>CH=CMe<sub>2</sub>), 4.96 (m, 1H; CH<sub>2</sub>CH<sub>2</sub>CH=CMe<sub>2</sub>), 6.49, 6.60 (m, 2H each; C<sub>5</sub>H<sub>4</sub>), 6.56 ppm (s, 5H; C<sub>5</sub>H<sub>5</sub>); <sup>13</sup>C{<sup>1</sup>H} NMR (100 MHz, CDCl<sub>3</sub>, 25 °C):  $\delta$  = 17.8, 23.4 (CH<sub>2</sub>CH<sub>2</sub>CH=CMe<sub>2</sub>), 25.9, 26.9 (CH<sub>2</sub>CH<sub>2</sub>CH=CMe<sub>2</sub>), 37.6 (CMe<sub>2</sub>), 47.3 (CpC), 118.8, 119.7, 148.9 (C<sub>5</sub>H<sub>4</sub>), 120.3 (C<sub>5</sub>H<sub>5</sub>), 124.3 (CH<sub>2</sub>CH<sub>2</sub>CH=CMe<sub>2</sub>), 131.8 ppm (CH<sub>2</sub>CH<sub>2</sub>CH=CMe<sub>2</sub>); FTIR (KBr):  $\tilde{\nu}$  = 1637 (C=C), 2854, 2924, 2963 (C<sub>ar</sub>-H), 3108 cm<sup>-1</sup> (C<sub>ar</sub>-H); EI-MS:  $m/z$  (%): 373 (11) [ $M^+$ +H], 337 (26) [ $M^+$ -Cl], 307 (28) [ $M^+$ -Cp], 300 (36) [ $M^+$ -2Cl+2H], 253 (63) [ $M^+$ -Ti-2Cl+H], 189 (29) [C<sub>5</sub>H<sub>4</sub>{CMe<sub>2</sub>CH<sub>2</sub>CH<sub>2</sub>CH=CMe<sub>2</sub>}<sup>+</sup>], 99 (65) [Cp+Cl-H], 69 (43) [2Cl-H]; elemental analysis calcd (%) for C<sub>19</sub>H<sub>26</sub>Cl<sub>2</sub>Ti (373.18 g mol<sup>-1</sup>): C 61.15, H 7.02; found: C 60.92, H 7.03.

**Synthesis of 18:** This compound was synthesised by using the same procedure as that described for **14**, with **6** (24.00 mL, 0.74 g, 2.88 mmol, 0.12 M in THF) and  $[Ti(\eta^5-C_5H_5)Cl_3]$  (0.61 g, 2.77 mmol). Yield: 0.74 g, 58%; <sup>1</sup>H NMR (400 MHz, CDCl<sub>3</sub>, 25 °C):  $\delta$  = 1.46, 1.64 (s, 3H each; CH<sub>2</sub>CH<sub>2</sub>CH=CMe<sub>2</sub>), 1.81 (s, 3H; CMePh), 1.98, 2.18 (m, 2H each; CH<sub>2</sub>CH<sub>2</sub>CH=CMe<sub>2</sub>), 5.05 (m, 1H; CH<sub>2</sub>CH<sub>2</sub>CH=CMe<sub>2</sub>), 6.04, 6.43 (m, 2H each; C<sub>5</sub>H<sub>4</sub>), 6.13 (s, 5H; C<sub>5</sub>H<sub>5</sub>), 6.87 (t, 1H;  $H_{para}$  of Ph ring), 7.27 (m, 2H;  $H_{meta}$  of Ph ring), 7.38 ppm (m, 2H;  $H_{ortho}$  of Ph ring); <sup>13</sup>C{<sup>1</sup>H} NMR (100 MHz, CDCl<sub>3</sub>, 25 °C):  $\delta$  = 17.8, 23.4 (CH<sub>2</sub>CH<sub>2</sub>CH=CMe<sub>2</sub>), 23.8, 25.9 (CH<sub>2</sub>CH<sub>2</sub>CH=CMe<sub>2</sub>), 43.8 (CMePh), 44.4 (CpC), 113.8 (CH<sub>2</sub>CH<sub>2</sub>CH=CMe<sub>2</sub>), 117.2, 122.4, 146.2 (C<sub>5</sub>H<sub>4</sub>), 120.8 (C<sub>5</sub>H<sub>5</sub>), 124.1, 129.9, 127.7, 128.6 (C<sub>6</sub>H<sub>5</sub>), 145.3 ppm (CH<sub>2</sub>CH<sub>2</sub>CH=CMe<sub>2</sub>); FTIR (KBr):  $\tilde{\nu}$  = 1672 (C=C), 2863, 2923, 2965 (C<sub>ar</sub>-H), 3054, 3104 cm<sup>-1</sup> (C<sub>ar</sub>-H); EI-MS:  $m/z$  (%): 435 (20) [ $M^+$ ], 399 (91) [ $M^+$ -Cl], 369 (41) [ $M^+$ -Cp], 251 (22) [C<sub>5</sub>H<sub>4</sub>{CMePhCH<sub>2</sub>CH<sub>2</sub>CH=CMe<sub>2</sub>}<sup>+</sup>], 181 (17) [ $M^+$ -C<sub>5</sub>H<sub>4</sub>{CMePhCH<sub>2</sub>CH<sub>2</sub>CH=CMe<sub>2</sub>}-H], 99 (100) [Cp+Cl+H], 91 (11) [C<sub>7</sub>H<sub>7</sub><sup>+</sup>], 69 (74) [2Cl-H]; elemental analysis calcd (%) for C<sub>24</sub>H<sub>28</sub>Cl<sub>2</sub>Ti (435.25 g mol<sup>-1</sup>): C 66.23, H 6.48; found: C 66.05, H 6.36.

**Synthesis of 19:** This compound was synthesised by using the same procedure as that described for **14**, with **5** (30 mL, 1.12 g, 5.70 mmol, 0.19 M in THF) and  $[TiCl_4(thf)_2]$  (0.95 g, 2.85 mmol). Yield: 0.16 g, 6%; <sup>1</sup>H NMR (400 MHz, CDCl<sub>3</sub>, 25 °C):  $\delta$  = 1.35 (s, 12H; CpCMe<sub>2</sub>), 1.42, 1.62 (m, 4H each; CH<sub>2</sub>CH<sub>2</sub>CH=CMe<sub>2</sub>), 1.47, 1.61 (s, 4H each; CH<sub>2</sub>CH<sub>2</sub>CH=CMe<sub>2</sub>), 4.94 (m, 2H; CH<sub>2</sub>CH<sub>2</sub>CH=CMe<sub>2</sub>), 6.43, 6.50 ppm (m, 4H each; C<sub>5</sub>H<sub>4</sub>); <sup>13</sup>C{<sup>1</sup>H} NMR (100 MHz, CDCl<sub>3</sub>, 25 °C):  $\delta$  = 17.8, 23.4 (CH<sub>2</sub>CH<sub>2</sub>CH=CMe<sub>2</sub>), 25.9, 26.8 (CH<sub>2</sub>CH<sub>2</sub>CH=CMe<sub>2</sub>), 37.6 (CMe<sub>2</sub>), 47.5 (CpC), 117.6, 120.3, 148.6 (C<sub>5</sub>H<sub>4</sub>), 124.6 (CH<sub>2</sub>CH<sub>2</sub>CH=CMe<sub>2</sub>), 131.7 ppm (CH<sub>2</sub>CH<sub>2</sub>CH=CMe<sub>2</sub>); FTIR (KBr):  $\tilde{\nu}$  = 1672 (C=C), 2864, 2921, 2965 (C<sub>ar</sub>-H), 3086, 3116 cm<sup>-1</sup> (C<sub>ar</sub>-H); EI-MS:  $m/z$  (%): 461 (68) [ $M^+$ -Cl], 377 (7) [ $M^+$ -Ti-2Cl-H], 189 (73)

[C<sub>5</sub>H<sub>4</sub>{CMe<sub>2</sub>CH<sub>2</sub>CH<sub>2</sub>CH=CMe<sub>2</sub>}<sup>+</sup>], 69 (100) [CH<sub>2</sub>CH=CMe<sub>2</sub>}<sup>+</sup>]; elemental analysis calcd (%) for C<sub>28</sub>H<sub>42</sub>Cl<sub>2</sub>Ti (497.41 g mol<sup>-1</sup>): C 67.61, H 8.51; found: C 67.22, H 8.43.

**Synthesis of 20:** This compound was synthesised by using the same procedure as that described for **14**, with **6** (26.00 mL, 0.80 g, 3.12 mmol, 0.12 M in THF) and [TiCl<sub>4</sub>(thf)<sub>2</sub>] (0.52 g, 1.56 mmol). Yield: 0.43 g, 22%; <sup>1</sup>H NMR (400 MHz, CDCl<sub>3</sub>, 25 °C, for the mixture of isomers): δ = 1.43, 1.44, 1.61, 1.62 (s, 6H each; CH<sub>2</sub>CH<sub>2</sub>CH=CMe<sub>2</sub>), 1.79 (s, 12H; CMePh), 1.70–2.20 (m, 16H; CH<sub>2</sub>CH<sub>2</sub>CH=CMe<sub>2</sub>), 5.03 (m, 4H; CH<sub>2</sub>CH<sub>2</sub>CH=CMe<sub>2</sub>), 5.16, 5.58, 6.07, 6.14, 6.27, 6.43, 6.51, 6.69 (m, 2H each; C<sub>5</sub>H<sub>4</sub>), 7.00–7.50 ppm (m, 20H; C<sub>6</sub>H<sub>5</sub>); <sup>13</sup>C{<sup>1</sup>H} NMR (100 MHz, CDCl<sub>3</sub>, 25 °C): δ = 17.7, 17.7, 23.1, 23.2 (CH<sub>2</sub>CH<sub>2</sub>CH=CMe<sub>2</sub>), 23.0, 24.0, 25.8, 25.8 (CH<sub>2</sub>CH<sub>2</sub>CH=CMe<sub>2</sub>), 42.3, 43.7 (CMePh), 44.4, 44.5 (CpC), 112.2, 115.9 (CH<sub>2</sub>CH<sub>2</sub>CH=CMe<sub>2</sub>), 117.8, 120.8, 120.8, 121.4, 122.9, 145.7, 145.9, 146.8, 147.0 (C<sub>5</sub>H<sub>4</sub>), 124.1, 124.3, 126.4, 126.5, 126.8, 127.5, 128.3, 128.3 (C<sub>6</sub>H<sub>5</sub>), 131.8, 131.8 ppm (CH<sub>2</sub>CH<sub>2</sub>CH=CMe<sub>2</sub>); FTIR (KBr): ν̄ = 1628 (C=C), 2874, 2928, 2966 (C<sub>al</sub>-H), 3064, 3101 cm<sup>-1</sup> (C<sub>ar</sub>-H); EI-MS: *m/z* (%): 585 (28) [M<sup>+</sup>-Cl], 369 (100) [M<sup>+</sup>-C<sub>5</sub>H<sub>4</sub>{CMePhCH<sub>2</sub>CH<sub>2</sub>CH=CMe<sub>2</sub>}<sup>+</sup>], 334 (17) [M<sup>+</sup>-C<sub>5</sub>H<sub>4</sub>{CMePhCH<sub>2</sub>CH<sub>2</sub>CH=CMe<sub>2</sub>}-Cl], 250 (47) [C<sub>5</sub>H<sub>4</sub>{CMePhCH<sub>2</sub>CH<sub>2</sub>CH=CMe<sub>2</sub>}<sup>+</sup>], 91 (68) [C<sub>7</sub>H<sub>7</sub><sup>+</sup>], 69 (89) [2Cl-H]; elemental analysis calcd (%) for C<sub>38</sub>H<sub>46</sub>Cl<sub>2</sub>Ti (621.54 g mol<sup>-1</sup>): C 73.43, H 7.46; found: C 72.64, H 7.22.

### Synthesis of materials incorporating the titanocene complexes (K11–K20)

A solution of the titanocene derivative (the quantity to obtain a theoretical level of 5% Ti/SiO<sub>2</sub>) in toluene (100 mL) was added to dehydrated KIT-6 (1.00 g) and the mixture was stirred overnight at 80 °C. The slurry was filtered through fritted discs and the solid residue was washed with toluene (5 × 200 mL). Finally, the resultant solid was dried under vacuum at room temperature for 24 h to give a pale-red, free-flowing powder.

**K11:** <sup>1</sup>H MAS NMR: δ = 2–3 (CMe<sub>2</sub>CH<sub>2</sub>CH<sub>2</sub>CH=CH<sub>2</sub>), 5–8 ppm (CMe<sub>2</sub>CH<sub>2</sub>CH<sub>2</sub>CH=CH<sub>2</sub>, C<sub>5</sub>H<sub>4</sub> and C<sub>5</sub>H<sub>5</sub>); <sup>13</sup>C CP MAS NMR: δ = 23, 27 (CMe<sub>2</sub>CH<sub>2</sub>CH<sub>2</sub>CH=CH<sub>2</sub>), 35 (CMe<sub>2</sub>CH<sub>2</sub>CH<sub>2</sub>CH=CH<sub>2</sub>), 112 (CMe<sub>2</sub>-CH<sub>2</sub>CH<sub>2</sub>CH=CH<sub>2</sub>), 118, 124, 127 (C<sub>5</sub>H<sub>4</sub> and C<sub>5</sub>H<sub>5</sub>), 138 ppm (CMe<sub>2</sub>-CH<sub>2</sub>CH<sub>2</sub>CH=CH<sub>2</sub>); <sup>29</sup>Si MAS NMR: δ = -111.5 (Q<sup>4</sup>), -102.9 (Q<sup>3</sup>), -93.9 ppm (Q<sup>2</sup>); FTIR (KBr): ν̄ = 801 (Si-OH), 1094 (Si-O-Si), 1383 (C-H bending), 1629 (physisorbed water), 2854, 2922, 2962 (C<sub>al</sub>-H stretching), and 3440 cm<sup>-1</sup> (O-H); Ti<sub>exp</sub> = 2.13%; S<sub>BET</sub> = 575 m<sup>2</sup> g<sup>-1</sup>; V<sub>p</sub> = 0.63 cm<sup>3</sup> g<sup>-1</sup>; D<sub>p</sub> = 63.6 Å.

**K12:** <sup>1</sup>H MAS NMR: δ = 2–3 (CMePhCH<sub>2</sub>CH<sub>2</sub>CH=CH<sub>2</sub>), 4–6.5 (CMePhCH<sub>2</sub>CH<sub>2</sub>CH=CH<sub>2</sub>, C<sub>5</sub>H<sub>4</sub> and C<sub>5</sub>H<sub>5</sub>), 7–8 ppm (CMePhCH<sub>2</sub>CH<sub>2</sub>CH=CH<sub>2</sub>); <sup>13</sup>C CP MAS NMR: δ = 18, 26 (CMePhCH<sub>2</sub>CH<sub>2</sub>CH=CH<sub>2</sub>), 38, 42 (CMePhCH<sub>2</sub>CH<sub>2</sub>CH=CH<sub>2</sub>), 115–120, 123–132 ppm (CMePhCH<sub>2</sub>CH<sub>2</sub>CH=CH<sub>2</sub>, C<sub>5</sub>H<sub>4</sub> and C<sub>5</sub>H<sub>5</sub>); <sup>29</sup>Si MAS NMR: δ = -112.6 (Q<sup>4</sup>), -104.9 (Q<sup>3</sup>), -92.3 ppm (Q<sup>2</sup>); FTIR (KBr): ν̄ = 457 (physisorbed water), 805 (Si-OH), 1080 (Si-O-Si), 1384 (C-H bending), 1629 (physisorbed water), 2857, 2926, 2963 (C<sub>al</sub>-H stretching), 3441 cm<sup>-1</sup> (O-H); Ti<sub>exp</sub> = 1.20%; S<sub>BET</sub> = 592 m<sup>2</sup> g<sup>-1</sup>; V<sub>p</sub> = 0.67 cm<sup>3</sup> g<sup>-1</sup>; D<sub>p</sub> = 63.7 Å.

**K13:** <sup>1</sup>H MAS NMR: δ = 2.5–6.5 (CMe<sub>2</sub>CH<sub>2</sub>CH<sub>2</sub>CH=CH<sub>2</sub>), 6–7 ppm (C<sub>5</sub>H<sub>4</sub>); <sup>13</sup>C CP MAS NMR: δ = 23, 27 (CMe<sub>2</sub>CH<sub>2</sub>CH<sub>2</sub>CH=CH<sub>2</sub>), 34 (CMe<sub>2</sub>CH<sub>2</sub>CH<sub>2</sub>CH=CH<sub>2</sub>), 44 (CMe<sub>2</sub>CH<sub>2</sub>CH<sub>2</sub>CH=CH<sub>2</sub>), 110, 115, 127 (CMe<sub>2</sub>CH<sub>2</sub>CH<sub>2</sub>CH=CH<sub>2</sub> and C<sub>5</sub>H<sub>4</sub>), 137 ppm (CMe<sub>2</sub>CH<sub>2</sub>CH<sub>2</sub>CH=CH<sub>2</sub>); <sup>29</sup>Si MAS NMR: δ = -112.1 (Q<sup>4</sup>), -103.7 (Q<sup>3</sup>), -92.0 ppm (Q<sup>2</sup>); FTIR (KBr): ν̄ = 458 (physisorbed water), 802 (Si-OH), 1077 (Si-O-Si), 1383 (C-H bending), 1635 (physisorbed water), 2859, 2926, 2965 (C<sub>al</sub>-H), 3431 cm<sup>-1</sup> (O-H); Ti<sub>exp</sub> = 2.17%; S<sub>BET</sub> = 610 m<sup>2</sup> g<sup>-1</sup>; V<sub>p</sub> = 0.68 cm<sup>3</sup> g<sup>-1</sup>; D<sub>p</sub> = 63.7 Å.

**K14:** <sup>1</sup>H MAS NMR: δ = 1.5–3 (CMePhCH<sub>2</sub>CH<sub>2</sub>CH=CH<sub>2</sub>), 4–6 (CMePhCH<sub>2</sub>CH<sub>2</sub>CH=CH<sub>2</sub>, and C<sub>5</sub>H<sub>4</sub>), 7–8 ppm (CMePhCH<sub>2</sub>CH<sub>2</sub>CH=CH<sub>2</sub>); <sup>13</sup>C CP MAS NMR: δ = 17, 30 (CMePhCH<sub>2</sub>CH<sub>2</sub>CH=CH<sub>2</sub>), 34, 40 (CMePhCH<sub>2</sub>CH<sub>2</sub>CH=CH<sub>2</sub>), 110–118, 125–140 ppm (CMePhCH<sub>2</sub>CH<sub>2</sub>CH=CH<sub>2</sub> and C<sub>5</sub>H<sub>4</sub>); <sup>29</sup>Si MAS NMR: δ = -111.9 (Q<sup>4</sup>), -103.4 (Q<sup>3</sup>), -91.8 ppm (Q<sup>2</sup>); FTIR (KBr): ν̄ = 454 (physisorbed water), 796 (Si-OH), 1079 (Si-O-Si), 1383 (C-H bending), 1636 (physisorbed water), 2923, 2973, 2986 (C<sub>al</sub>-H), 3431 cm<sup>-1</sup> (O-H); Ti<sub>exp</sub> = 2.26%; S<sub>BET</sub> = 469 m<sup>2</sup> g<sup>-1</sup>; V<sub>p</sub> = 0.42 cm<sup>3</sup> g<sup>-1</sup>; D<sub>p</sub> = 68.7 Å.

**K15:** <sup>1</sup>H MAS NMR: δ = 0–1 (SiMe<sub>3</sub>), 2.5–7.5 ppm (CMe<sub>2</sub>CH<sub>2</sub>CH<sub>2</sub>CH=CH<sub>2</sub>, C<sub>5</sub>H<sub>3</sub> and C<sub>5</sub>H<sub>5</sub>); <sup>13</sup>C CP MAS NMR: δ = -2.6 (SiMe<sub>3</sub>), 24, 27, 31 (CMe<sub>2</sub>CH<sub>2</sub>CH<sub>2</sub>CH=CH<sub>2</sub>), 40 (CMe<sub>2</sub>CH<sub>2</sub>CH<sub>2</sub>CH=CH<sub>2</sub>), 117, 126, 131, 144 ppm (CMe<sub>2</sub>CH<sub>2</sub>CH<sub>2</sub>CH=CH<sub>2</sub>, C<sub>5</sub>H<sub>3</sub> and C<sub>5</sub>H<sub>5</sub>); <sup>29</sup>Si MAS NMR: δ = -112.4 (Q<sup>4</sup>), -103.7 (Q<sup>3</sup>), -91.9 ppm (Q<sup>2</sup>); FTIR (KBr): ν̄ = 457 (physisorbed water), 796 (Si-OH), 1082 (Si-O-Si), 1383 (C-H bending), 1621 (physisorbed water), 2925, 2933, 2970 (C<sub>al</sub>-H), 3434 cm<sup>-1</sup> (O-H); Ti<sub>exp</sub> = 3.06%; S<sub>BET</sub> = 561 m<sup>2</sup> g<sup>-1</sup>; V<sub>p</sub> = 0.44 cm<sup>3</sup> g<sup>-1</sup>; D<sub>p</sub> = 63.8 Å.

**K16:** <sup>1</sup>H MAS NMR: δ = 0–1 (SiMe<sub>3</sub>), 2–4 (CMePhCH<sub>2</sub>CH<sub>2</sub>CH=CH<sub>2</sub>), 6–8 ppm (CMePhCH<sub>2</sub>CH<sub>2</sub>CH=CH<sub>2</sub>, C<sub>5</sub>H<sub>3</sub> and C<sub>5</sub>H<sub>5</sub>); <sup>13</sup>C CP MAS NMR: δ = -3.4 (SiMe<sub>3</sub>), 26, 37, 42, 47 (CMePhCH<sub>2</sub>CH<sub>2</sub>CH=CH<sub>2</sub>), 117, 127 ppm (CMePhCH<sub>2</sub>CH<sub>2</sub>CH=CH<sub>2</sub>, C<sub>5</sub>H<sub>3</sub> and C<sub>5</sub>H<sub>5</sub>); <sup>29</sup>Si MAS NMR: δ = -112.4 (Q<sup>4</sup>), -103.4 (Q<sup>3</sup>), -92.1 ppm (Q<sup>2</sup>); FTIR (KBr): ν̄ = 456 (physisorbed water), 805 (Si-OH), 1079 (Si-O-Si), 1383 (C-H bending), 1636 (physisorbed water), 2924, 2963 (C<sub>al</sub>-H), 3431 cm<sup>-1</sup> (O-H); Ti<sub>exp</sub> = 2.43%; S<sub>BET</sub> = 532 m<sup>2</sup> g<sup>-1</sup>; V<sub>p</sub> = 0.59 cm<sup>3</sup> g<sup>-1</sup>; D<sub>p</sub> = 64.3 Å.

**K17:** <sup>1</sup>H MAS NMR: δ = 1–4.5 (CMe<sub>2</sub>CH<sub>2</sub>CH<sub>2</sub>CH=CMe<sub>2</sub>), 4.5–6.5 ppm (CMe<sub>2</sub>CH<sub>2</sub>CH<sub>2</sub>CH=CMe<sub>2</sub>, C<sub>5</sub>H<sub>4</sub> and C<sub>5</sub>H<sub>5</sub>); <sup>13</sup>C CP MAS NMR: δ = 14, 21, 22 (CMe<sub>2</sub>CH<sub>2</sub>CH<sub>2</sub>CH=CMe<sub>2</sub>), 34 (CMe<sub>2</sub>CH<sub>2</sub>CH<sub>2</sub>CH=CMe<sub>2</sub>), 60 (CMe<sub>2</sub>CH<sub>2</sub>CH<sub>2</sub>CH=CMe<sub>2</sub>), 112, 128, 135, 156, 165 ppm (CMe<sub>2</sub>CH<sub>2</sub>CH<sub>2</sub>CH=CMe<sub>2</sub>, C<sub>5</sub>H<sub>4</sub> and C<sub>5</sub>H<sub>5</sub>); <sup>29</sup>Si MAS NMR: δ = -112.5 (Q<sup>4</sup>), -103.0 (Q<sup>3</sup>), -92.4 ppm (Q<sup>2</sup>); FTIR (KBr): ν̄ = 456 (physisorbed water), 800 (Si-OH), 1081 (Si-O-Si), 1383 (C-H bending), 1636 (physisorbed water), 2854, 2922, 2971 (C<sub>al</sub>-H), 3432 cm<sup>-1</sup> (O-H); Ti<sub>exp</sub> = 2.23%; S<sub>BET</sub> = 492 m<sup>2</sup> g<sup>-1</sup>; V<sub>p</sub> = 0.44 cm<sup>3</sup> g<sup>-1</sup>; D<sub>p</sub> = 64.3 Å.

**K18:** <sup>1</sup>H MAS NMR: δ = 1–3.5 (CMePhCH<sub>2</sub>CH<sub>2</sub>CH=CMe<sub>2</sub>), 4.5–7 (CMePhCH<sub>2</sub>CH<sub>2</sub>CH=CMe<sub>2</sub>, C<sub>5</sub>H<sub>4</sub> and C<sub>5</sub>H<sub>5</sub>), 7–8.5 ppm (CMePhCH<sub>2</sub>CH<sub>2</sub>CH=CMe<sub>2</sub>); <sup>13</sup>C CP MAS NMR: δ = 11, 23, 27, 33 (CMePhCH<sub>2</sub>CH<sub>2</sub>CH=CMe<sub>2</sub>), 57 (CMePhCH<sub>2</sub>CH<sub>2</sub>CH=CMe<sub>2</sub>), 117, 124, 141 ppm (CMePhCH<sub>2</sub>CH<sub>2</sub>CH=CMe<sub>2</sub>, C<sub>5</sub>H<sub>4</sub> and C<sub>5</sub>H<sub>5</sub>); <sup>29</sup>Si MAS NMR: δ = -112.1 (Q<sup>4</sup>), -102.6 (Q<sup>3</sup>), -92.1 ppm (Q<sup>2</sup>); FTIR (KBr): ν̄ = 456 (physisorbed water), 801 (Si-OH), 1081 (Si-O-Si), 1419 (C-H bending), 1636 (physisorbed water), 2854, 2922, 2971 (C<sub>al</sub>-H), 3431 cm<sup>-1</sup> (O-H); Ti<sub>exp</sub> = 2.00%; S<sub>BET</sub> = 442 m<sup>2</sup> g<sup>-1</sup>; V<sub>p</sub> = 0.41 cm<sup>3</sup> g<sup>-1</sup>; D<sub>p</sub> = 63.9 Å.

**K19:** <sup>1</sup>H MAS NMR: δ = 1.5–3.5 (CMe<sub>2</sub>CH<sub>2</sub>CH<sub>2</sub>CH=CMe<sub>2</sub>), 4.5–6.5 ppm (CMe<sub>2</sub>CH<sub>2</sub>CH<sub>2</sub>CH=CMe<sub>2</sub> and C<sub>5</sub>H<sub>4</sub>); <sup>13</sup>C CP MAS NMR: δ = 15, 19, 23 (CMe<sub>2</sub>CH<sub>2</sub>CH<sub>2</sub>CH=CMe<sub>2</sub>), 34 (CMe<sub>2</sub>CH<sub>2</sub>CH<sub>2</sub>CH=CMe<sub>2</sub>), 63 (CMe<sub>2</sub>-CH<sub>2</sub>CH<sub>2</sub>CH=CMe<sub>2</sub>), 114, 127, 134, 162, 168 ppm (CMe<sub>2</sub>CH<sub>2</sub>CH<sub>2</sub>CH=CMe<sub>2</sub> and C<sub>5</sub>H<sub>4</sub>); <sup>29</sup>Si MAS NMR: δ = -112.0 (Q<sup>4</sup>), -102.1 (Q<sup>3</sup>), -92.6 ppm (Q<sup>2</sup>); FTIR (KBr): ν̄ = 456 (physisorbed water), 798 (Si-OH), 1082 (Si-O-Si), 1387 (C-H bending), 1636 (physisorbed water), 2925, 2972 (C<sub>al</sub>-H), 3444 cm<sup>-1</sup> (O-H); Ti<sub>exp</sub> = 2.43%; S<sub>BET</sub> = 365 m<sup>2</sup> g<sup>-1</sup>; V<sub>p</sub> = 0.37 cm<sup>3</sup> g<sup>-1</sup>; D<sub>p</sub> = 63.9 Å.

**K20:** <sup>1</sup>H MAS NMR: δ = 1–4 (CMePhCH<sub>2</sub>CH<sub>2</sub>CH=CMe<sub>2</sub>), 4–6.5 (CMePhCH<sub>2</sub>CH<sub>2</sub>CH=CMe<sub>2</sub> and C<sub>5</sub>H<sub>4</sub>), 7–8 ppm (CMePhCH<sub>2</sub>CH<sub>2</sub>CH=CMe<sub>2</sub>); <sup>13</sup>C CP MAS NMR: δ = 11–57 (CMePhCH<sub>2</sub>CH<sub>2</sub>CH=CMe<sub>2</sub>), 117, 124, 141 ppm (CMePhCH<sub>2</sub>CH<sub>2</sub>CH=CMe<sub>2</sub> and C<sub>5</sub>H<sub>4</sub>); <sup>29</sup>Si MAS NMR: δ = -112.3 (Q<sup>4</sup>), -102.1 (Q<sup>3</sup>), -92.9 ppm (Q<sup>2</sup>); FTIR (KBr): ν̄ = 456 (physisorbed water), 801 (Si-OH), 1082 (Si-O-Si), 1383 (C-H bending), 1636 (physisorbed water), 2934, 2978 (C<sub>al</sub>-H), 3431 cm<sup>-1</sup> (O-H); Ti<sub>exp</sub> = 4.85%; S<sub>BET</sub> = 348 m<sup>2</sup> g<sup>-1</sup>; V<sub>p</sub> = 0.33 cm<sup>3</sup> g<sup>-1</sup>; D<sub>p</sub> = 64.2 Å.

## In vitro studies

**Cell cultures:** Biological evaluations were performed in vitro with the following cell lines: A2780 human ovary carcinoma, MCF-7 human breast adenocarcinoma, DLD-1 colon carcinoma and HEK-293 human normal epithelial kidney cell lines; these were acquired from the European Collection of Cell Cultures through Sigma Aldrich Company (St Louis, Missouri, USA).

A2780 and DLD-1 cell lines were cultivated in RPMI-1640 culture medium supplemented with 2 mM glutamine and 10% foetal bovine serum (FCS); MCF-7 cells required minimum essential medium eagle (MEM) with 2 mM glutamine, 1% non-essential amino acids (NEA) and 10% FCS, and for 293 cell line cultivation we used Dulbecco's modified eagle medium with 2 mM glutamine, 1% NEA and 10% FCS; all culture media and nutrients were obtained from Sigma Aldrich.

Cells were cultivated under sterile conditions by using a CO<sub>2</sub> Series incubator from Uniequip GmbH (Planegg, Germany) at a constant temperature of 37 °C and 5% CO<sub>2</sub> in cell culture flasks. The cell passages were made at subconfluency with enzymatic methods by using 0.25% trypsin ethylenediaminetetraacetic acid (EDTA; from Sigma). Cell viability was evaluated microscopically through Trypan Blue staining.

General instrumentation used for cell cultures were as follows: R320 centrifuge with a swing-out rotor from Hettich (Tuttingen, Germany), a Sartorius analytical scale (Goettingen, Germany), a Heto Ultra Freeze –80 °C freezer (Heto Holten, Allerød, Denmark), an MVE Cryosystem 2000 liquid nitrogen tank (MVE Cryogenics, Ball Ground, GA, USA), a CKX41 inverted-phase fluorescence microscope (Olympus, Hamburg, Germany), and a Titramax 1000 shaker with incubator (Heidolph, Schwabach, Germany).

**Cytotoxicity:** Compounds were dissolved in DMSO (from Fluka Chemie, Bichs, Switzerland). The dilutions of solvent used were tested on the four cell lines for their toxicity and the results were negative. The final concentrations of the compounds were in the range of 0.3–1500 μM and for the materials we used concentrations between 1 and 2500 μg mL<sup>-1</sup>.

To assess the cytotoxicity of the compounds, we used the colourimetric MTT cell viability assay, which is an optimised method of determining viable cell number in proliferation and cytotoxicity studies.<sup>[76]</sup> This test is based on the cleavage of the yellow thiazolyl blue tetrazolium bromide salt (MTT) to form a water-soluble blue formazan product by mitochondrial enzymes of the living cells. Thus, the amount of formazan produced is directly proportional to the number of viable cells present during MTT exposure.

The cells were plated on 96-well Nunclon TC cell culture microplates (Nalgene Nunc, through Thermo Scientific Company, Waltham, MA, USA), at a 2 × 10<sup>4</sup> cell/well density in 200 μL of media. After 24 h, incubation cells were treated with the serial dilution of compounds in triplicate. For every compound, colour controls were used, by treating wells containing cell culture media only (without cells). As a viability control, we used the untreated cells, and oxaliplatin (Oxaliplatin Accord, Accord Healthcare Ltd, North Harrow, Great Britain) was the cytostatic reference drug. Oxaliplatin was diluted in phosphate buffered saline solution (PBS, Sigma Aldrich); the concentrations used were in the 0.01–100 μM range.

The spectrophotometric measurements were made by using a Synergy 2 microplate reader (BioTek Instruments, Winooski, VT, USA) at λ = 492 nm. The cells were subjected to titanocene derivate and material action for 24 h.

**Apoptosis evaluation:** For apoptosis assay, a flow cytometric evaluation was performed. Cells were plated on six-well multi-dishes

(from Nunc, Thermo Scientific) at a concentration of 5 × 10<sup>5</sup> cells mL<sup>-1</sup> media, and incubated for 24 h to obtain a well-attached 80–90% confluent population. They were treated for 8 h with a final concentration above their IC<sub>50</sub> values of the compounds: 50 μM titanocenes in the cell culture media, 500 μg mL<sup>-1</sup> titanocene-containing nanomaterials and 25 μM oxaliplatin; concentrations were proportional to their IC<sub>50</sub> (or M<sub>50</sub>) values and they were chosen to exhibit an effect after just 8 h of treatment. After treatment, the cells were detached from the plate, washed and re-suspended in PBS.

We employed the Alexa Fluor 488 Annexin V/PI Apoptosis Kit for flow cytometry, a Molecular Probes product (Eugene, OR, USA), following the manufacturer's indications. This method distinguished the apoptotic cells within a population, based on characteristic morphological and biochemical changes, one of which was the translocation of phosphatidylserine (PS) on the cell membrane outer leaflet. The Alexa Fluor labelled Annexin V binds to PS located on the cell outer surface, and this confers a photostable green colouration to the apoptotic cells, which is detectable at λ = 488 nm by the flow cytometer. In addition, propidium iodide (PI), a nucleic acid binding dye, penetrated inside the dead cells and indicated the viability of the population. After treatment with the two dyes, cells were subjected to flow cytometry measurement by using a method described earlier.<sup>[77]</sup> The two colourations were quantified and depicted by using the histograms of the FACS Canto equipment (Beckton, Dickinson and Company, Franklin Lakes, NJ, USA).

**Cell signalling:** The expression of apoptosis-related molecules Bcl-xL and Bax-α were evaluated quantitatively with the enzyme-linked immunosorbent assay (ELISA). For this purpose, cells were treated in the same manner as those for the apoptosis assay; as a reference we used untreated control cells. We used a final concentration derived from IC<sub>50</sub> (or M<sub>50</sub>) values of the compounds: 20 μM titanocenes in the cell culture media, 200 μg mL<sup>-1</sup> titanocene-containing materials and 10 μM oxaliplatin. Samples were subjected to lysis in FNN0011 cell extraction buffer (from Molecular Probes, Eugene, OR, USA) on ice. Cell lysates were centrifuged at 2000 rpm and aliquots of supernatant were prepared for the tests. The protein concentration in cell lysates was measured by the Bradford method,<sup>[78]</sup> using a UV/Vis spectrophotometer (Jasco Analytical Instruments, Easton, MD, USA). All samples were adjusted to a protein concentration of 50 μg mL<sup>-1</sup> by dilution in PBS.

The DuoSet intracellular human total Bcl-xL ELISA kit and the DuoSet intracellular human total Bax-α ELISA kit were from R&D Systems (Minneapolis, MN, USA); reagents were employed according to the manufacturer's indications. All experiments were performed in duplicate. Colourimetric measurements were performed on a Sunrise Elisa reader and an automated plate washer (both from Tecan, Männedorf, Germany). The standard values provided by the pure recombinant human Bax-α and Bcl-xL proteins allowed the Magellan software to draw the calibration curve and to compute the concentration of relevant proteins from each well.

**PARP inhibitory capacity:** The PARP inhibitory capacity of new compounds was assessed by using the HT Universal Colourimetric PARP assay kit with histone-coated strip wells from Trevigen Incorporation (Gaithersburg, MD, USA). For this purpose, the studied compounds were diluted in PARP buffer; we used a range of 10–150 mg mL<sup>-1</sup> final concentration/well interval for **15**, **20**, **K15** and **K20**, and we used two different wells for each concentration. The capacity of the synthesised compounds to inhibit PARP-HSA enzyme activity was compared with the reference, 3-aminobenzamide, provided by the kit. PARP-1 activity modulation of the new compounds was tested by measuring the biotinylated poly-ADP-

ribose on histone proteins from the microplate surface. This accumulation is proportional with the magnitude of PARP-1 cleavage, and can be measured colourimetrically.

**PARP-1 cleavage in treated cells:** The PARP activity in cell extracts during apoptosis was assessed by using the HT Colourimetric PARP Apoptosis Assay Kit (Trevigen), which also included histone-coated well strips. We used the cell lysates obtained from treated and untreated cell, as described earlier, in the amount of 25  $\mu\text{L}$ /well. In this experiment, lysates from **K15** and **K20** were utilised; all measurements were made in duplicate. The baseline sample, before apoptosis, for each cell line was considered as the untreated cell batch. As a reference, we used etoposide, which was a cytostatic drug provided by the kit. Cells were treated with etoposide as follows: 20  $\mu\text{M}$  for A2780 and MCF-7 cell line, whereas for DLD-1 we used a final concentration of 50  $\mu\text{M}$ . The PARP inhibitory activity of each compound was determined semi-quantitatively based on poly-ADP-ribose deposited on the plate and visualised by anti-PARP monoclonal antibody binding.

In both methods the enzyme concentration increase was monitored by TACS-Sapphire colourimetric substrate and measured with the Synergy 2 microplate reader.

**Cellular titanium uptake:** For cellular uptake of titanocene compounds and materials, the malignant cells (A2780, MCF-7 and DLD-1) were cultivated on 25  $\text{cm}^2$  Nunclon delta surface culture flasks for 24 h and after total attachment of the cells to surface, at 70–80% subconfluency, they were treated with the studied compounds, at the concentrations of 500  $\mu\text{M}$  compounds and 500  $\mu\text{g mL}^{-1}$  materials. The final concentration of Ti in the cell culture media was 23.91  $\mu\text{g mL}^{-1}$  for **15** and 23.90  $\mu\text{g mL}^{-1}$  for **20**, whereas for the materials the Ti concentration in the cell environment was 15.3  $\mu\text{g mL}^{-1}$  in **K15** and 24.25  $\mu\text{g mL}^{-1}$  in **K20**. After 24 h, treatment cells were collected by trypsinisation in centrifuge tubes; supernatant was also collected to recover the detached cells. After gentle centrifugation, cell counting and two washes with PBS, cell pellets were counted immediately and frozen in cryotubes at  $-70^\circ\text{C}$ ; every sample contained  $10^6$  cells suspended in PBS (200  $\mu\text{L}$ ). The compounds and materials had the ability to attach themselves to the cell surface, with very strong bonds, and even after repeated washing the pellets were visibly coloured because of the presence of the compounds not only on their outer membrane, but inside the cell.

Quantification of the titanium content was performed by ICP-AES by using a Varian Vista AX Pro Varian 720-ES instrument.

**Study of titanium release:** The titanium release of the materials under biological conditions was performed in a blood simulating fluid. This consisted of a pH 7.4 buffer prepared according to previously reported procedures.<sup>[79]</sup> In duplicate, 1 mL of simulated blood fluid was added to 10 mg of the studied materials (this ratio was used to guarantee that the quantity associated with the release of 1% Ti was within the detection limits of the inductively coupled plasma atomic emission spectrometer). The suspensions were incubated at  $37^\circ\text{C}$  in a water bath for different time periods up to 72 h. Afterwards, the suspension was subsequently filtered and the filtrate was analysed by ICP-AES by using a Varian Vista AX Pro Varian 720-ES instrument.

## Acknowledgements

We gratefully acknowledge financial support from the Ministerio de Economía y Competitividad, Spain (grant no. CTQ2012-30762); the Romanian National Authority for Scientific Re-

search (grant no. PN-II-ID-PCE-2011-3-1057) supported the evaluation of the biological activity of the compounds and materials.

**Keywords:** antitumour agents · apoptosis · cytotoxicity · mesoporous materials · titanium

- [1] See, for example: I. Ali, W. A. Wani, K. Saleem, A. Haque, *Anticancer Agents Med. Chem.* **2013**, *13*, 296–306.
- [2] C. G. Hartinger, P. J. Dyson, *Chem. Soc. Rev.* **2009**, *38*, 391–401.
- [3] P. C. A. Bruijninx, P. J. Sadler, *Adv. Inorg. Chem.* **2009**, *61*, 1–62.
- [4] C.-H. Zhou, Y.-Y. Zhang, C.-Y. Yan, K. Wan, L.-L. Gan, Y. Shi, *Anticancer Agents Med. Chem.* **2010**, *10*, 371–395.
- [5] S. Komeda, A. Casini, *Curr. Top. Med. Chem.* **2012**, *12*, 219–235.
- [6] E. Meléndez, *Inorg. Chim. Acta* **2012**, *393*, 36–52.
- [7] C. Nardon, G. Boscutti, D. Fregona, *Anticancer Res.* **2014**, *34*, 487–492.
- [8] C. Sanchez-Cano, M. J. Hannon, *Dalton Trans.* **2009**, *48*, 10702–10711.
- [9] S. Gómez-Ruiz, *New Directions in the Fight against Cancer: From Metal Complexes to Nanostructured Materials, in Molecules at Work: Self-Assembly, Nanomaterials, Molecular Machinery* (Ed.: B. Pignataro), Wiley-VCH, Weinheim, **2012**.
- [10] A. R. Kennedy, A. J. Florence, F. J. McInnes, N. J. Wheate, *Dalton Trans.* **2009**, *37*, 7695–7700.
- [11] C. C. L. Pereira, C. V. Diogo, A. Burgeiro, P. J. Oliveira, M. P. M. Marques, S. S. Braga, F. A. A. Paz, M. Pillinger, I. S. Gonçalves, *Organometallics* **2008**, *27*, 4948–4956.
- [12] A. M. Krause-Heuer, N. J. Wheate, M. J. Tilby, D. G. Pearson, C. J. Ottley, J. R. Aldrich-Wright, *Inorg. Chem.* **2008**, *47*, 6880–6888.
- [13] D. Plazuk, A. Vessières, E. A. Hillard, O. Buriez, E. Labbé, P. Pigeon, M.-A. Plamont, C. Amatore, J. Zakrzewski, G. Jaouen, *J. Med. Chem.* **2009**, *52*, 4964–4967.
- [14] M. Galanski, B. K. Keppler, *Anticancer Agents Med. Chem.* **2007**, *7*, 55–73.
- [15] E. Allard, C. Passirani, E. Garcion, P. Pigeon, A. Vessières, G. Jaouen, J. P. Benoit, *J. Control. Release* **2008**, *130*, 146–153.
- [16] S. Dhar, L. Zhuang, J. Thomale, H. Dai, S. J. Lippard, *J. Am. Chem. Soc.* **2008**, *130*, 11467–11476.
- [17] A. A. Bhirde, V. Patel, J. Gavard, G. Zhang, A. A. Sousa, A. Masedunskas, R. D. Leapman, R. Weigert, J. S. Gutkind, J. F. Rusling, *ACS Nano* **2009**, *3*, 307–316.
- [18] S. Dhar, F. X. Gu, R. Langer, O. C. Farokhzad, S. J. Lippard, *Proc. Natl. Acad. Sci. USA* **2008**, *105*, 17356–17361.
- [19] J. M. Dominguez-Vera, *J. Inorg. Biochem.* **2004**, *98*, 469–472.
- [20] See, for example: B. Therrien, G. Suess-Fink, P. Govindaswamy, A. K. Renfrew, P. J. Dyson, *Angew. Chem.* **2008**, *120*, 3833–3836; *Angew. Chem. Int. Ed.* **2008**, *47*, 3773–3778.
- [21] K. Ajima, T. Murakami, Y. Mizoguchi, K. Tsuchida, T. Ichihashi, S. Iijima, M. Yudasaka, *ACS Nano* **2008**, *2*, 2057–2064.
- [22] R. P. Feazell, N. Nakayama-Ratchford, H. Dai, S. J. Lippard, *J. Am. Chem. Soc.* **2007**, *129*, 8438–8439.
- [23] B. W. Harper, A. M. Krause-Heuer, M. P. Grant, M. Manohar, K. B. Garbutcheon-Singh, J. R. Aldrich-Wright, *Chem. Eur. J.* **2010**, *16*, 7064–7077.
- [24] W. J. Rieter, K. M. Pott, K. M. L. Taylor, W. Lin, *J. Am. Chem. Soc.* **2008**, *130*, 11584–11585.
- [25] A. Nguyen, V. Marsaud, C. Bouclier, S. Top, A. Vessières, P. Pigeon, R. Gref, P. Legrand, G. Jaouen, J.-M. Renoir, *Int. J. Pharm.* **2008**, *347*, 128–135.
- [26] W. Zhu, Y. L. Li, L. X. Liu, W. L. Zhang, Y. M. Chen, F. Xi, *J. Biomed. Mater. Res.* **2011**, *96A*, 330–340.
- [27] A. Salinas, P. Esbrit, M. Vallet-Regí, *Biomater. Sci.* **2013**, *1*, 40–51.
- [28] M. Colilla, B. González, M. Vallet-Regí, *Biomater. Sci.* **2013**, *1*, 114–134.
- [29] A. J. Salinas, M. Vallet-Regí, *RSC Adv.* **2013**, *3*, 11116–11131.
- [30] B. Palazzo, M. Iafisco, M. Laforgia, N. Margiotta, G. Natile, C. L. Bianchi, D. Walsh, S. Mann, N. Roveri, *Adv. Funct. Mater.* **2007**, *17*, 2180–2188.
- [31] M. Iafisco, B. Palazzo, M. Marchetti, N. Margiotta, R. Ostuni, G. Natile, M. Morpurgo, V. Gandin, C. Marzano, N. Roveri, *J. Mater. Chem.* **2009**, *19*, 8385–8392.
- [32] C. Y. Lai, B. G. Trewyn, D. M. Jeftinija, K. Jeftinija, S. Xu, S. Jeftinija, V. S. Lin, *J. Am. Chem. Soc.* **2003**, *125*, 4451–4459.

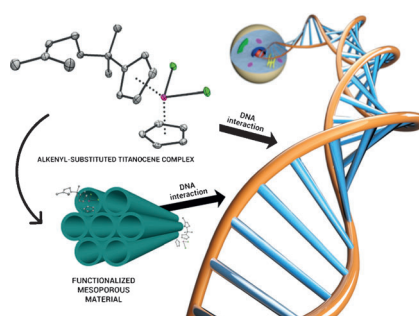
- [33] D. Pérez-Quintanilla, S. Gómez-Ruiz, Ž. Žižak, Z. D. Juranić, I. Sierra, S. Prashar, I. del Hierro, M. Fajardo, G. N. Kaluderović, *Chem. Eur. J.* **2009**, *15*, 5588–5597.
- [34] G. N. Kaluderović, D. Pérez-Quintanilla, I. Sierra, S. Prashar, I. del Hierro, Ž. Žižak, Z. D. Juranić, M. Fajardo, S. Gómez-Ruiz, *J. Mater. Chem.* **2010**, *20*, 806–814.
- [35] G. N. Kaluderović, D. Pérez-Quintanilla, Ž. Žižak, Z. D. Juranić, S. Gómez-Ruiz, *Dalton Trans.* **2010**, *39*, 2597–2608.
- [36] A. García-Peñas, S. Gómez-Ruiz, D. Pérez-Quintanilla, R. Paschke, I. Sierra, S. Prashar, I. del Hierro, G. N. Kaluderović, *J. Inorg. Biochem.* **2012**, *106*, 100–110.
- [37] K. Strohfeltd, M. Tacke, *Chem. Soc. Rev.* **2008**, *37*, 1174–1187.
- [38] S. Gómez-Ruiz, D. Maksimović-Ivanić, S. Mijatović, G. N. Kaluderović, *Bioinorg. Chem. Appl.* **2012**, 140284.
- [39] S. Gómez-Ruiz, G. N. Kaluderović, D. Polo-Cerón, S. Prashar, M. Fajardo, Ž. Žižak, Z. D. Juranić, T. J. Sabo, *Inorg. Chem. Commun.* **2007**, *10*, 748–752.
- [40] J. Ceballos-Torres, S. Gómez-Ruiz, G. N. Kaluderović, M. Fajardo, R. Paschke, S. Prashar, *J. Organomet. Chem.* **2012**, *700*, 188–193.
- [41] J. Ceballos-Torres, M. J. Caballero-Rodríguez, S. Prashar, R. Paschke, D. Steinborn, G. N. Kaluderović, S. Gómez-Ruiz, *J. Organomet. Chem.* **2012**, *716*, 201–207.
- [42] S. Gómez-Ruiz, D. Polo-Cerón, S. Prashar, M. Fajardo, A. Antiñolo, A. Otero, *Eur. J. Inorg. Chem.* **2007**, 4445–4455.
- [43] S. Gómez-Ruiz, G. N. Kaluderović, D. Polo-Cerón, V. Tayurskaya, S. Prashar, M. Fajardo, R. Paschke, *J. Organomet. Chem.* **2009**, *694*, 3032–3038.
- [44] S. Gómez-Ruiz, G. N. Kaluderović, Ž. Žižak, I. Besu, Z. D. Juranić, S. Prashar, M. Fajardo, *J. Organomet. Chem.* **2009**, *694*, 1981–1987.
- [45] F. Kleitz, S. H. Choi, R. Ryoo, *Chem. Commun.* **2003**, 2136–2137.
- [46] K. S. W. Sing, D. H. Everett, R. A. W. Haul, L. Moscou, R. A. Pierotti, J. Rouquérol, T. Siemieniowska, *Pure Appl. Chem.* **1985**, *57*, 603–620.
- [47] T. W. Kim, F. Kleitz, B. Paul, R. Ryoo, *J. Am. Chem. Soc.* **2005**, *127*, 7601–7610.
- [48] C. V. Christodolou, A. G. Eliopoulos, L. S. Young, L. Hodgkins, D. R. Ferry, D. J. Kerr, *Br. J. Cancer* **1996**, *77*, 2088–2097.
- [49] P. W. Causey, M. C. Baird, S. P. C. Cole, *Organometallics* **2004**, *23*, 4486–4494.
- [50] O. R. Allen, A. L. Gott, J. A. Hartley, J. M. Hartley, R. J. Knox, P. C. McGowan, *Dalton Trans.* **2007**, 5082–5090.
- [51] M. Tacke, L. T. Allen, L. Cuffe, W. M. Gallagher, L. Ying, O. Mendoza, H. Muller-Bunz, F. J. K. Rehmann, N. Sweeney, *J. Organomet. Chem.* **2004**, *689*, 2242–2249.
- [52] G. D. Potter, M. C. Baird, S. P. C. Cole, *J. Organomet. Chem.* **2007**, *692*, 3508–3518.
- [53] C. M. Manna, O. Braitbard, E. Weiss, J. Hochman, E. Y. Tshuva, *ChemMedChem* **2012**, *7*, 703–708.
- [54] M. Wenzel, B. Bertrand, M. J. Eymen, V. Comte, J. A. Harvey, P. Richard, M. Groessl, O. Zava, H. Amrouche, P. D. Harvey, P. Le Gendre, M. Picquet, A. Casini, *Inorg. Chem.* **2011**, *50*, 9472–9480.
- [55] X. Stachtea, N. Karamanos, N. Klouras, *Anticancer Res.* **2009**, *29*, 3227–3231.
- [56] L. M. Gao, E. Meléndez, *Met. Based Drugs* **2010**, *2010*, 286–298.
- [57] L. M. Gao, J. L. Vera, J. Matta, E. Meléndez, *J. Biol. Inorg. Chem.* **2010**, *15*, 851–859.
- [58] M. Napoli, C. Saturnino, E. Sirignano, A. Popolo, A. Pinto, P. Longo, *Eur. J. Med. Chem.* **2011**, *46*, 122–128.
- [59] P. Beckova, O. Oberschmidt, A. R. Hanousck, C. Pampillón, V. Schirrmacher, N. J. Sweeney, K. Strohfeltd, M. Tacke, *Anticancer Drugs* **2007**, *18*, 311–315.
- [60] J. Schur, C. M. Manna, A. Deally, R. W. Köster, M. Tacke, E. Y. Tshuva, I. Ott, *Chem. Commun.* **2013**, *49*, 4785–4787.
- [61] C. Riccardi, I. Nicoletti, *Nat. Protoc.* **2006**, *1*, 1458–1461.
- [62] P. N. Kelly, A. Strasser, *Cell Death Differ.* **2011**, *18*, 1414–1424.
- [63] C. Gao, A. Y. Wang, *J. Histochem. Cytochem.* **2009**, *57*, 1139–1148.
- [64] A. C. Tsamandas, D. Kardamakis, T. Petsas, V. Zolota, V. Vassiliou, T. Matatsoris, H. Kalofonos, C. E. Vagianos, C. D. Scopa, *In Vivo* **2007**, *21*, 113–118.
- [65] S. Kagawa, J. Gu, T. Honda, T. J. McDonnell, S. G. Swisher, J. A. Roth, B. Fang, *Clin. Cancer Res.* **2001**, *7*, 1474–1480.
- [66] A. Aranovich, Q. Liu, T. Collins, F. Geng, S. Dixit, B. Leber, D. W. Andrews, *Mol. Cell* **2012**, *45*, 754–763.
- [67] P. J. Beale, P. Rogers, F. Boxall, S. Y. Sharp, L. R. Kelland, *Br. J. Cancer* **2000**, *82*, 436–440.
- [68] Y. Edden, S. D. Wexner, M. Berho, *Colorectal Dis.* **2012**, *14*, 555–561.
- [69] H. M. Amm, T. Zhou, A. D. Steg, H. Kuo, Y. Li, D. J. Buchsbaum, *Mol. Cancer Res.* **2011**, *9*, 403–417.
- [70] T. V. Bagnyukova, I. G. Serebriiskii, Y. Zhou, E. A. Hopper-Borge, E. A. Golemis, I. Astsaturov, *Cancer Biol. Ther.* **2010**, *10*, 839–853.
- [71] X. Luo, W. L. Kraus, *Genes Dev.* **2012**, *26*, 417–432.
- [72] J. Sand-Dejmek, G. Adelmant, B. Sobhian, A. S. Calkins, J. Marto, D. J. Iglehart, J. B. Lazaro, *Mol. Cancer* **2011**, *10*, 74.
- [73] S. Aizawa, K. Ookawa, T. Kudo, J. Asano, M. Hayakari, S. Tsuchida, *Cancer Sci.* **2003**, *94*, 886–893.
- [74] G. Zhu, P. Chang, S. J. Lippard, *Biochemistry* **2010**, *49*, 6177–6183.
- [75] S. Gómez-Ruiz, G. N. Kaluderović, S. Prashar, D. Polo-Cerón, M. Fajardo, Ž. Žižak, T. J. Sabo, Z. D. Juranić, *J. Inorg. Biochem.* **2008**, *102*, 1558–1570.
- [76] P. W. Sylvester, *Methods Mol. Biol.* **2011**, *716*, 157–168.
- [77] A. D. Goodrich, A. Ersek, N. M. Varain, D. Groza, M. Cenariu, D. S. Thain, G. Almeida-Porada, C. D. Porada, F. D. Zanjan, *Exp. Hematol.* **2010**, *38*, 516–525.
- [78] G. A. Filip, I. D. Postescu, C. Tatomir, A. Muresan, S. Clichici, *J. Physiol. Pharmacol.* **2012**, *63*, 423–432.
- [79] P. Horcajada, A. Rámila, J. Pérez-Pariente, M. Vallet-Regí, *Microporous Mesoporous Mater.* **2004**, *68*, 105–109.
- [80] CCDC-983057 (17) and 983058 (18) contain the supplementary crystallographic data for this paper. These data can be obtained free of charge from The Cambridge Crystallographic Data Centre via [www.ccdc.cam.ac.uk/data\\_request/cif](http://www.ccdc.cam.ac.uk/data_request/cif).

Received: January 24, 2014

Published online on ■ ■ ■ ■, 0000

## FULL PAPER

**Concealed activity:** A series of titanocene-functionalized silica-based materials have been synthesized, characterized, and studied in vitro against human cell lines (see figure). They act as Trojan horses for the incorporation of the titanium active species into cells, leading to much higher quantities of titanium uptake in cells, changing the dynamics of apoptotic morphological and functional changes, and inducing programmed cell death in tumor cell populations.



### Drug Delivery

*J. Ceballos-Torres, P. Virag, M. Cenariu, S. Prashar, M. Fajardo, E. Fischer-Fodor,\* S. Gómez-Ruiz\**



**Anti-cancer Applications of Titanocene-Functionalised Nanostructured Systems: An Insight into Cell Death Mechanisms**

